ČESKÉ VYSOKÉ UČENÍ TECHNICKÉ V PRAZE

FAKULTA STROJNÍ

ÚSTAV MATERIÁLOVÉHO INŽENÝRSTVÍ

DIPLOMOVÁ PRÁCE

Vlastnosti nástřiků wolframu deponovaných technologií RF-ICP

Properties of RF-ICP sprayed tungsten coatings

AUTOR: Lukáš Babka

STUDIJNÍ PROGRAM: Výrobní inženýrství

VEDOUCÍ PRÁCE: doc. Ing. Jan Čížek Ph.D.

PRAHA 2023

ZADÁNÍ DIPLOMOVÉ PRÁCE

I. OSOBNÍ A STUDIJNÍ ÚDAJE

Příjmení: **Babka** Jméno: **Lukáš** Osobní číslo: **483136**

Fakulta/ústav: **Fakulta strojní**

Zadávající katedra/ústav: **Ústav materiálového inženýrství**

Studijní program: **Výrobní inženýrství**

Specializace: **Bez specializace**

II. ÚDAJE K DIPLOMOVÉ PRÁCI

Název diplomové práce:

Vlastnosti nástřiků wolframu deponovaných technologií RF-ICP

Název diplomové práce anglicky:

Properties of RF-ICP sprayed tungsten coatings

Pokyny pro vypracování:

1. Vypracovat rešerši o problematice jaderné fúze a základních charakteristikách technologie RF-ICP.
2. Nanést zvolené prášky W za různých hodnot depozičních parametrů pomocí RF-ICP.
3. Provést analýzy mikrostruktury a tepelné vodivosti deponovaných nástřiků.

Seznam doporučené literatury:

1. Davis: Handbook of Thermal Spray Technology. ASM International, 2004.
2. Boulos: New frontiers in thermal plasmas from space to nanomaterials. Nuclear Engineering and Technology, 44, 2012, 1.
3. Kovarik, Xue, Fan, Boulos: RF plasma deposition of refractory metals: Case study for tungsten. Proceedings of 2006 International Thermal Spray Conference, 2003, 215.
4. Kovarik, Fan, Boulos: In flight properties of W particles in an Ar-H2 plasma. Journal of Thermal Spray Technology, 16, 2007, 229.
5. Kovarik, Cizek, Klecka, Karlik, Capek, Siegl, Chraska, Takayasu: Mechanical properties and fatigue crack growth in tungsten deposited by RF-plasma. Surface and Coatings Technology, 410, 126930.
6. Matejicek, Chraska, Linke: Thermal Spray Coatings for Fusion Applications-Review. Journal of Thermal Spray Technology, 16, 2007, 64.

Jméno a pracoviště vedoucí(ho) diplomové práce:

doc. Ing. Jan Čížek, Ph.D. Ústav materiálového inženýrství

Jméno a pracoviště druhé(ho) vedoucí(ho) nebo konzultanta(ky) diplomové práce:

Datum zadání diplomové práce: **23.03.2023** Termín odevzdání diplomové práce: **31.07.2023**

Platnost zadání diplomové práce: _____

doc. Ing. Jan Čížek, Ph.D. podpis vedoucí(ho) práce	doc. Ing. Ladislav Cvrček, Ph.D. podpis vedoucí(ho) ústavu/katedry	doc. Ing. Miroslav Španiel, CSc. podpis děkana(ky)

III. PŘEVZETÍ ZADÁNÍ

Diplomant bere na vědomí, že je povinen vypracovat diplomovou práci samostatně, bez cizí pomoci, s výjimkou poskytnutých konzultací. Seznam použité literatury, jiných pramenů a jmen konzultantů je třeba uvést v diplomové práci.

Datum převzetí zadání _____ Podpis studenta _____

Prohlášení

Prohlašuji, že jsem tuto práci vypracoval samostatně, a to výhradně s použitím pramenů a literatury uvedených v seznamu citovaných zdrojů.

V Praze dne: …… …….

Podpis

Anotace

Tato diplomová práce popisuje využití technologie radiofrekvenčního indukčně vázaného plazmatu pro deponování nástřiků wolframu na ocelové substráty. Cílem experimentální části práce bylo optimalizovat proces a nanést kvalitní nástřiky W na připravené ocelové substráty pro možnou budoucí fúzní aplikaci. Vyhodnocení vzorků bylo provedeno analýzou na elektronovém mikroskopu ve spolupráci s Ústavem fyziky plazmatu Akademie věd České republiky. Byla hodnocena zejména závislost zvolených depozičních parametrů na vlastnosti deponovaných nástřiků, jako například jejich tloušťku, porozitu, či míru výskytu nenatavených částic. Získané výsledky byly následně diskutovány a porovnány s dostupnou literaturou.

Klíčová slova

jaderná fúze, wolfram, žárové nanášení, RF-ICP, radiofrekvenční indukčně vázané plazma

Annotation

This diploma thesis is focused on the usage of inductively-coupled plasma technology for the deposition of W coatings on steel substrates. The experimental part of the work aimed to optimize the process and apply high-quality W coatings on prepared AISI 304 steel substrates for potential fusion applications. The evaluation of the samples was carried out by electron microscope analysis in cooperation with the Institute of Plasma Physics of the Academy of Sciences of the Czech Republic. The influence of the selected process parameters on the properties of the deposited coatings, such as their thickness, porosity or unmelted particles content, was observed. The obtained results were then discussed and compared with the literature.

Keywords

nuclear fusion, tungsten, flame spray, RF-ICP, inductively-coupled plasma

Poděkování

Rád bych poděkoval vedoucímu mé diplomové práce doc. Ing. Janu Čížkovi, Ph.D. za odborný a trpělivý přístup, a především cenné rady a připomínky. Dále pak děkuji Ing. Jakubovi Klečkovi za významnou pomoc při přípravě vzorků a jejich následném vyhodnocení a Ing. Janu Medřickému, Ph.D. za pomoc spojenou s analýzou vstupních materiálů. Děkuji též své přítelkyni a rodině za neskomírající podporu během studia. Bez Vás bych to nezvládl.

Table of content

1 Introduction

Nuclear fusion is certainly one of the most important discoveries of the 20th century and offers a promising alternative to nuclear fission. It represents a clean, sustainable energy source using a commonly available and nearly inexhaustible fuel source.

However, the path to mastering nuclear fusion is complicated, and the material solution for the internal components of fusion reactors is one of today's most difficult engineering challenges. These materials must withstand conditions that no material has had to face. These are, e.g., extreme temperatures, pressures, thermal shocks, and radiation. For this reason, developing a solid and financially sustainable solution is a crucial step in the progress of harnessing the nuclear fusion.

In the past, for example, the CFC composite appeared to be promising, but it was unfortunately shown to be susceptible to plasma erosion and thus to the risk of failure. Currently, several materials are under development for applications in fusion reactors.

Tungsten appears to be a good solution, as its properties suit perfectly for fusion applications. Initially, this element was considered as unsuitable due to the sputtering of its ionized atoms into the plasma. However, this problem was solved by a tailored design solution of the divertor. For the moment, tungsten is planned to be used in the form of coatings, as deposition of the coatings is a possible way to enhance the durability of the PFC (plasma facing components). There is a minimum required thickness for these coatings, and thus the use of methods such as PVD (physical vapor deposition) and CVD (chemical vapor deposition) appears economically unacceptable. Consequently, thermal spray methods come into play, such as the RF-ICP (radiofrequency inductively-coupled plasma) method used in this thesis. This method can deposit the coatings in a protective atmosphere and thus prevent their oxidation while delivering sufficient power to process materials with high melting temperatures, such as tungsten.

In the thesis, the theory of nuclear fusion is first briefly described, while the emphasis is placed mainly on the materials used for internal reactor components. In the second part of the literature review, thermal spray is presented, with the methods using plasma as a heat source for melting the additive material described in more detail. A special emphasis is then placed on the RF-ICP technology, used at the Institute of Plasma Physics in Prague for the first time in Czech Republic. In the experimental part of the thesis, the deposition details of the protective tungsten coatings using this technology are described, as are the details of the final coatings analyses. In the end, the influence of four selected application parameters on the properties of the coatings is discussed.

2 Literature research

2.1 Nuclear fusion

2.1.1 General introduction

The sun has been warming our planet for billions of years. This star provides us energy in the form of electromagnetic radiation from nuclear fusion – the process of fusing hydrogen nuclei into helium and other heavier elements. Here, the reaction takes place on an enormous scale – 600 million tons of hydrogen are burned up every second, which is, however, a negligible amount compared to the size of this star [1]. It would be sufficient to manage the reaction only in a fraction of this amount to safely ensure the energy consumption of mankind and increase the overall comfort of life.

Nuclear fusion was first mentioned by scientists Paneth and Peters in 1926 [1] [2]. It was first considered an energy source 8 years later by E. Rutherford, M. L. E. Oliphant and P. Harteck, who in 1934 successfully demonstrated the fusion of two deuterium nuclei [3]. This fundamental discovery started a long era of research with the aim to conquer fusion and thus provide us with an essentially inexhaustible energy source. However, for a long time, it was uncertain whether it was possible to ignite and sustain fusion reaction in Earth conditions. This was until 1997, when the JET (Joint European Torus) fusion reactor achieved a fusion power of 16 MW while being supplied by a power of 24 MW [3] [4]. Since 1998, the successor to this project has been ITER (International Thermonuclear Experimental Reactor), on which experts from the EU, Japan, the Russian Federation, the USA, China and South Korea are currently working. The primary mission of the ITER project is not the commercial production of energy. Instead, it is primarily intended to describe the reactor physics precisely enough so that operational engineers can safely take over the control of the reaction. At the same time, it should serve to verify and optimize the possibility of tritium production directly in the reactor chamber. The scientific knowledge obtained throughout this project should then be used for a better understanding of nuclear fusion and, ideally, for constructing the first fusion power plants. The first fusion power plant, which is already planned for electricity production, is the DEMO (Demonstration fusion reactor) project.

Nuclear fusion promises high process purity while using commonly available, virtually inexhaustible fuel, deuterium and tritium. Deuterium is simply obtained by electrolysis of sea water, and tritium, although rarely found freely on Earth, can be relatively easily obtained by reacting neutrons with a commonly available alkali metal – lithium. This reaction is planned to take place directly inside the fusion reactor. The oceans contain approximately 4.76×10^{16} kg of deuterium and 2.44×10^{14} kg of lithium, which according to preliminary calculations, will provide humanity's energy needs for 8 billion years. In comparison with the estimated lifespan of the Sun (5.3 billion years), it can perhaps be stated that the fusion will cover humanity energetically until the end of the Solar System [3]. Therefore, fusion can be considered the ideal successor to fossil fuels, for which optimistic estimates predict a supply for the next tens or, at most, hundreds of years [1].

At the same time, fusion is a very safe and clean energy source. In our conditions, there is no possibility of a spontaneous explosion of the fusion fuel, and the reactor contains only gram amounts. In the first generations of fusion reactors, the energy carriers are high-energy neutrons causing secondary radioactivity in the internal reactor components. However, only a small volume of the materials will be affected; in the future, neutron-free fusion is being considered, significantly suppressing the secondary radioactivity [5]. The "waste" product of the fusion reaction is the inert gas helium, which is currently expensively obtained as a by-product during natural gas extraction or by isolating from minerals. The easy acquisition of this product thus opens up possibilities for the development of new industries (e.g., the use of airships in the autonomous transport of goods) and, at the same time, will make the processes in which it is commonly used cheaper (e.g., magnetic resonance or magnesium welding [6]. Finally, nuclear fusion outperforms renewable energy sources, as it is independent of the weather, unlike, for example, photovoltaic power plants.

Above all, these properties are crucial due to the increasing energy consumption, pressure on ecology, and the economy of energy production processes, thus determining fusion as a highly prospective energy source. However, the many advantages are also accompanied with many problems that currently hinder the possibility of putting fusion reactors into operation.

2.1.2 Principle of the nuclear fusion

Unlike nuclear fission, which is used in, for example, fission reactors, the essence of nuclear fusion is the directly opposite phenomenon, i.e., instead of fission of atoms, they fuse. In Figure 1, it can be seen that energy is released if the nuclei of elements lighter than iron fuse. Figure 1 also shows many times higher fusion efficiency compared to nuclear fission.

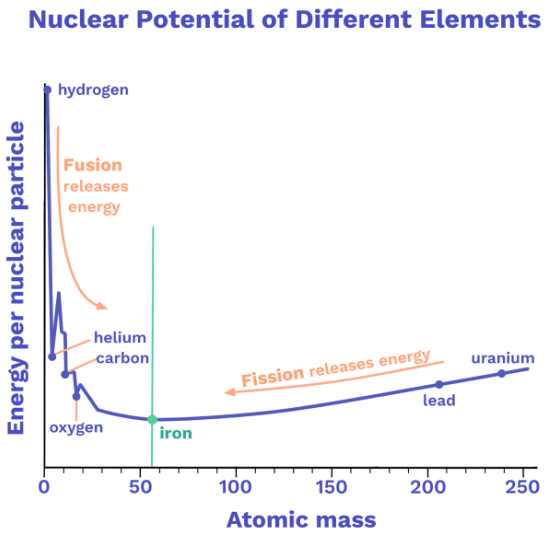

Figure 1: Diagram of the amount of energy released during fission/fusion as a function of the number of nucleons in the atomic nuclei [7].

However, nuclear fusion can only occur under certain conditions. The desired phenomenon is the fusion of atomic nuclei, containing only neutrons and protons, and therefore having the same electric charge. The same electric charge causes them to be strongly repelled by the electrostatic force and to achieve their fusion, the nuclei must gain sufficient energy to overcome the electrostatic barrier. At the moment of overcoming this barrier, the repulsive electric force ceases to act, and the attractive nuclear force begins to prevail. The repulsive force of equally charged nuclei can be overcome either by their mutual collision at a sufficient speed, given to them by a suitable accelerator, or by heating them to the so-called ignition temperature. For industrial use in energetics, heating to the ignition temperature is chosen as the most convenient method, as in the case of accelerating the particles, unwanted electrical (Coulombic) collisions are more likely to occur than the required nuclear collisions [1].

There are several candidates of fusion reactions. Most current fusion devices work with the fusion reaction of two nuclei of heavy hydrogen, i.e., deuterium. However, to achieve a positive energy gain, it is technologically easier to carry out a reaction of heavy and superheavy hydrogen, i.e., deuterium and tritium, as is shown in Figure 2 [4].

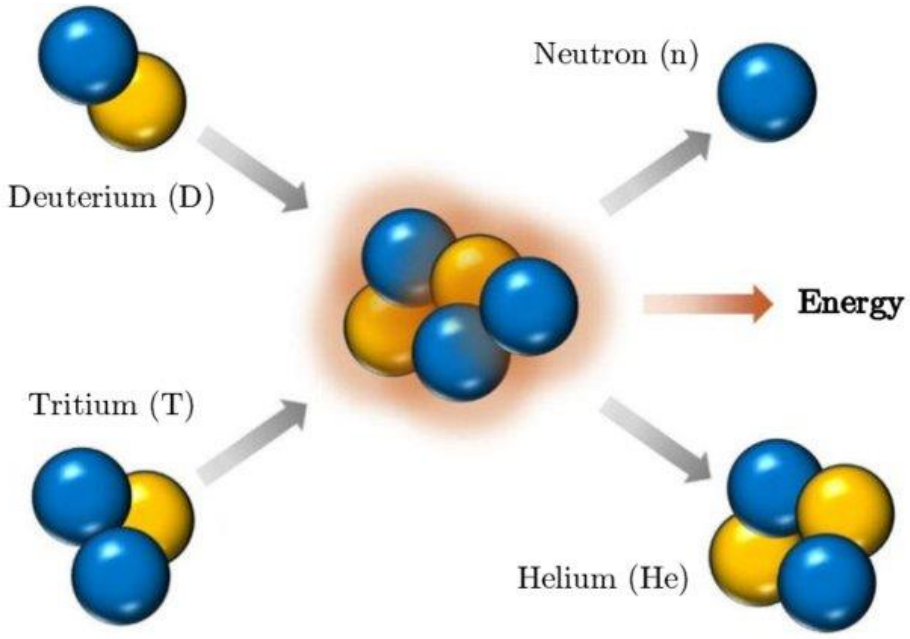

Figure 2: A simplified scheme of the fusion reaction of deuterium and tritium [8].

The reaction of deuterium with tritium has a conveniently low ignition temperature compared to other types of fusion reactions and these are therefore planned as the input elements for the first generation of fusion reactors. Deuterium is planned to be supplied as raw input material, and the reaction of lithium with neutrons would then release tritium. The ongoing reaction of deuterium and tritium produces positive helium nuclei (alpha particles) and neutrons. The alpha particles continuously heat the plasma, and the neutrons react with a special material covering the chamber, the so-called "breeder blanket", in which they react with lithium-6 to form tritium. Both reactions are summarized in Equation 1.

D	**+**	**^{6}Li**	**→**	**2 ^{4}He**	**+**			**22,4**	**MeV**
D	+	T	→	^{4}He	+	n	+	17,6	MeV
^{6}Li	+	n	→	^{4}He	+	T	+	4,8	MeV

(1)

The heat from the reaction of neutrons with lithium-6 can then be considered the output of a future fusion power plant. The moment when the energy supplied by alpha particles is sufficient to heat the plasma and the fusion generates more energy than what is needed to start it is called the fusion ignition, and such fusion reaction can then be called spontaneous [9].

The conditions for fusion ignition were described in 1955 by the British scientist J. D. Lawson. It is a relationship between the temperature and density of atomic nuclei and the minimum time the nuclei remain at this temperature and density. The so-called Lawson criterion sets the minimum parameters for achieving nuclear fusion with a positive energy balance and has the general form:

$$\eta\tau_E \geq f(T), \tag{2}$$

where η represents the density of atomic nuclei, or the number of particles per cubic meter, τ_E represents the energy confinement time of the atomic nuclei, i.e., the rate of energy leakage from the plasma, and T represents the temperature of the nuclei. In Figure 3, it is possible to observe the equilibrium and ignition curves for the reaction of deuterium with tritium. It is clear that the optimal temperature ensuring the easiest energy gain (i.e., fusion ignition) is approximately 160 million degrees K. At this temperature, all matter is already in a fully ionized plasma state; in other words, it is a mixture of positively charged nuclei and electrons [1] [4] [10].

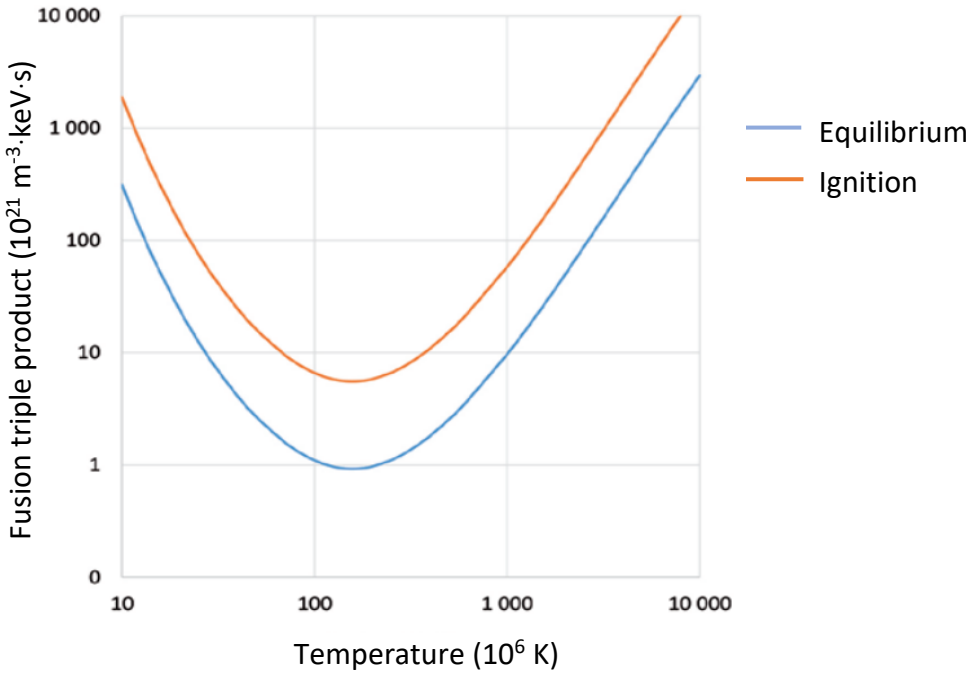

Figure 3: Lawson's criterion for the fusion reaction of deuterium and tritium [3].

Lawson's criterion suggests two primary ways of obtaining a positive energy balance – with a high density of atomic nuclei and a short confinement time, this is the inertial confinement [1]. With a low density of atomic nuclei (in the order of 10^{20} m^{-3}) and a longer confinement time, this is the magnetic confinement. The principle of the inertial confinement method is used, for example, in hydrogen bombs. However, its use in the energy sector is technologically too demanding at the moment, as it involves very rapid heating of the fuel and its subsequent ignition, where the inertia of the fuel prevents its immediate escape. The fusion power plant would then have to work on repeating these miniature explosions, which is technically too complicated. Therefore, magnetic confinement is currently the closest to the real application. Several experimental fusion devices allow plasma to be held magnetically. Among the most important concepts are tokamaks, stellarators, or magnetic pinches. However, according to interim results, tokamak is the hottest candidate for future industrial use.

2.1.3 Tokamak

This originally Russian concept saw the light of day in 1950 when scientists I. Sakharov and I. Tamm designed a prototype of a toroid-shaped container with a transformer core, which was seated inside electromagnetic coils. The construction took place in 1955, while the first tokamak was officially named TMP – a torus with a magnetic field. It was basically a vacuum ceramic container. In 1958, the concept was reworked into an all-metal chamber without any insulation breaks [11] [12]. The supremacy of tokamaks was then completed in 1970 when all experimental fusion systems were rebuilt in the form of a tokamak [1].

The shape of this device is a so-called toroid, created by rotating a circle or ellipse around an axis located outside the surface of this geometric element. The first tokamaks used a circular cross-section of the chamber, but over time, the cross-section changed to the shape of the letter "D". In the magnetic confinement method, plasma particles are held using magnetic fields in which the Lorentz force acts on the particles. This causes electrons and ions to move around the magnetic field lines in a circle. A suitable shape of the magnetic fields and a pressure balance between the plasma and the magnetic fields will then cause the plasma to be kept at a certain distance from the walls of the chamber structure [3].

In principle, tokamak is a rather simple solution, where the transformer core (central superconducting solenoid) is surrounded by a toroidal chamber with a double lining filled with hydrogen gas (Figure 4), while plasma flows inside the chamber. The first layer of lining for application in state-of-the-art systems (especially in ITER) consists of beryllium protective tiles anchored to a supporting structure made of corrosion-resistant steel. This layer then covers the entire chamber area, except for the divertor. For the future experimental fusion reactor of the DEMO type WCLL (water cooled lithium lead), replaceable modules made of ferritic-martensitic EUROFER steel containing channels for the flow of a mixture of lead and lithium is considered as a solution for the construction of the blanket. Lithium is planned to be used to produce tritium for its own D-T reaction inside the chamber. Coolant, most often water, flows between the first and the second layers. At the bottom of the chamber is a divertor (Figure 4), having a primary function of the removal of gases from the fusion reaction. At the same time,

it is the area with the most significant thermal stress. The chamber is housed inside superconducting magnets, which are sealed in a vacuum cryostat [1] [4].

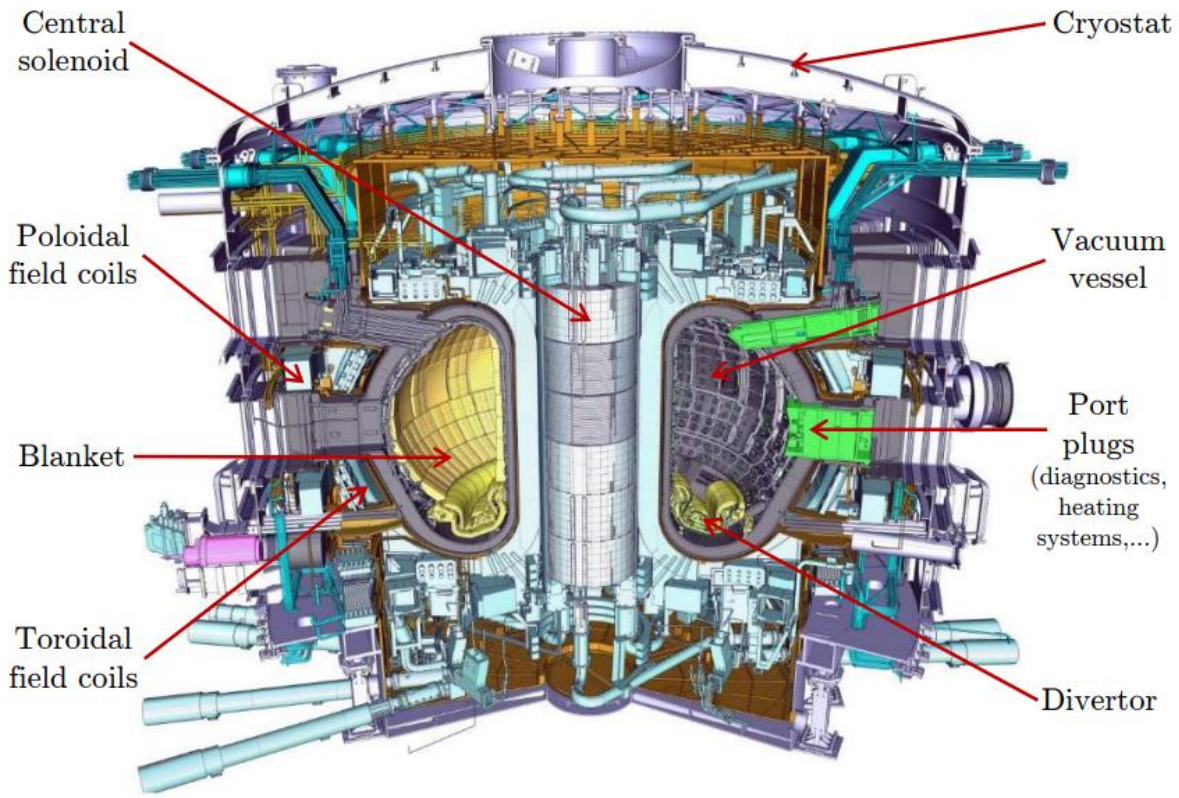

Figure 4: Main internal components of ITER tokamak (image courtesy of EFDA).

For describing this device, it is convenient to introduce two main directions for easier understanding. The toroidal direction follows the axis of the chamber ring, and the poloidal direction lies in a plane perpendicular to the toroidal direction and follows a circle centered on the axis describing the toroidal direction. Both directions are visualized in Figure 5.

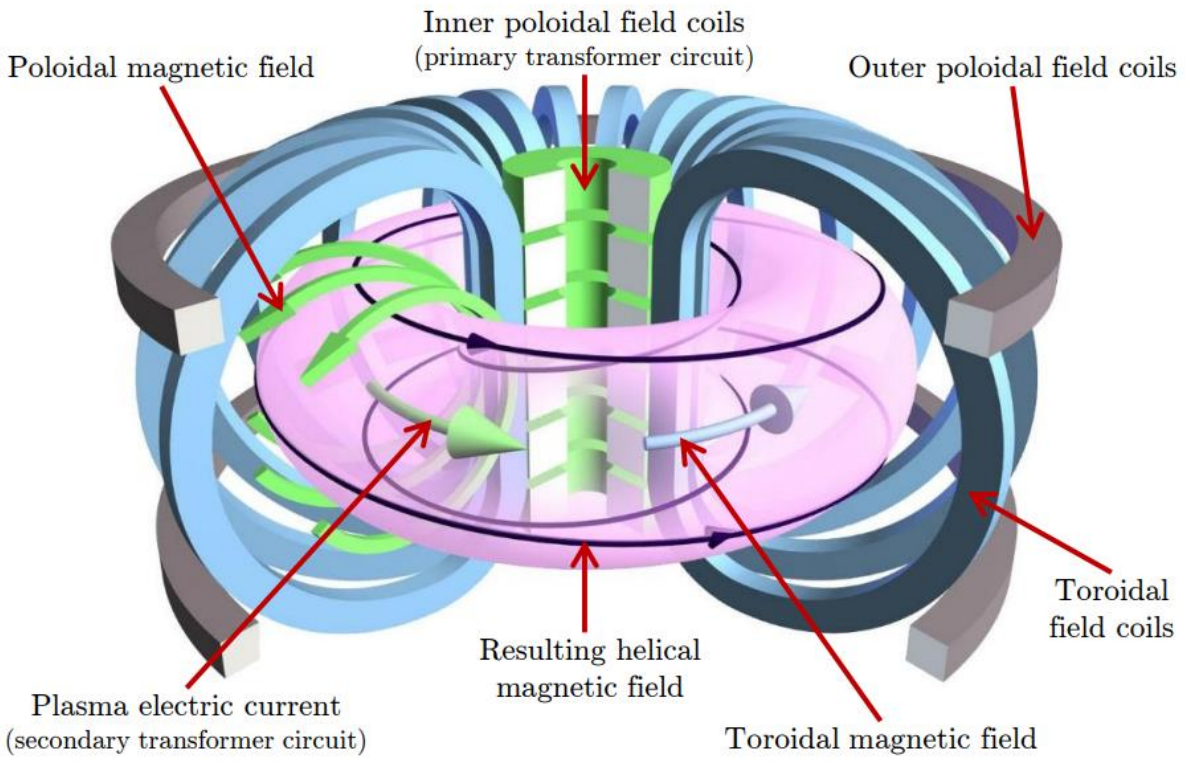

Figure 5: Visualization of the main magnetic fields of tokamak (image courtesy of EFDA).

Consequently, two main magnetic fields are introduced – toroidal and poloidal. The toroidal field is generated by coils that are wound around the entire circumference of the vacuum chamber. The poloidal field is generated by a strong magnetic current that is induced by a central solenoid inside the plasma. The combination of these two magnetic fields creates a magnetic field in the shape of a helix (a helical magnetic field), which keeps the plasma inside the chamber. At the same time, the helical magnetic field helps suppress the so-called toroidal drift of charged particles, which is a phenomenon resulting from the inhomogeneity of magnetic fields and centrifugal force [1]. Lately, with the increasing perfection of the magnetic insulation, the time for which the plasma can be held magnetically also increases.

The heating of the plasma inside the tokamak takes place in two phases. Heating to a temperature of approximately 5×10^7 °C takes place with the help of a current induced inside the plasma, where the considerable electrical resistance of hydrogen gas is used. This is heating by the so-called Joule heat, which is created when the electric current passes through a conductor; in this case, the plasma. This is one of the most significant advantages of tokamaks compared to competing stellarators, as their biggest disadvantage is the problematic heating of the plasma at lower temperatures. Above this temperature, the efficiency of plasma heating drops sharply as its electrical resistance decreases. In the second phase, it is necessary to provide additional heating in a way that does not depend on the electrical resistance of the plasma. There are currently two solutions. The first is the so-called radio frequency method, where radio frequency waves with the cyclotron frequency of electrons or plasma ions are used. These waves are generated outside the reactor and subsequently brought to the reactor

using waveguides. Antennas are then placed Inside of the reactor, which transmit the waves directly into the plasma. At the same time, it is possible to partially remove certain instabilities in the plasma by appropriately directing the radio waves. The second option is the NBI method, i.e., heating neutral beams. This heating method consists in injecting neutral deuterium particles (neutral means that they can reach the center of the plasma without being deflected by the magnetic field) or other hydrogen isotopes directly into the plasma. These particles subsequently transfer their kinetic energy through collisions and further heat the plasma. Currently, a combination of these two plasma heating methods is used [1] [3] [4].

Although the plasma is held magnetically inside the vacuum vessel without a physical contact, the internal reactor components are still exposed to enormous temperatures, heat fluxes and shocks, and radiation. These components are referred to as PFCs, i.e., plasma facing components; the following chapter will be devoted to them.

2.1.4 PFC

The material choice and design of the so-called plasma-facing components undoubtedly belong among the most complex engineering challenges. The materials inside the reactor must withstand extreme conditions. Among the most significant degradation factors are for example high heat fluxes and thermal shocks resulting from abnormalities within the plasma, plasma erosion, or radiation damage. For that reason, high demands are placed on these materials, while the availability of primary raw materials and the economy of the entire solution must also be considered when choosing suitable materials. At the same time, it is necessary to consider the design of the components themselves. From the point of view of the fusion device operation, an appropriate location of the used structural elements is vital, for example for refueling, servicing or diagnosing the conditions inside the reactor [13].

The following aspects must be considered when solving the design and choosing the material for the PFC [14] [15]:

- Significant heat fluxes (in the planned DEMO fusion power plant in the area of the divertor, the nominal value of the flux for the first wall is set at 0.5 MW/m^2 and plasma instability peaks are up to tens of GW/m^2)
- Damage to components due to erosion by plasma, fusion neutrons, and plasma particles (there is a gradual degradation of the material, the aim is to minimize this phenomenon and, at the same time, suppress plasma contamination by material particles)
- Material compatibility with the plasma (especially abnormalities in the plasma generate large electromagnetic forces)
- Appropriate structural design
- Price

Currently, materials with a high melting point, thermal conductivity and heat resistance, such as tungsten, are used. CFC carbon composites were used in the past, but they were eventually rejected due to their high hydrogen retention and susceptibility to erosion. As discussed in section 2.3, in ITER, the first layer is made of beryllium tiles and the divertor is

protected by tungsten. In fact, the use of tungsten was not previously considered, mainly due to its large atomic number and the fact that its atoms emit intense X-rays when ionized. However, this problem was solved by preventing the sputtering of ionized tungsten atoms from the divertor into the plasma. Tungsten also does not absorb tritium and has a higher resistance to plasma erosion than beryllium, making it one of the hottest candidates for further research of the PFC protection [1] [13].

2.2 Tungsten

Tungsten was discovered at the end of the 18th century by the Swedish chemist Carl Wilhelm Scheel. It is a gray to silvery-white metal with the highest melting point of all metallic elements. It has a very high density of 19.25 g/cm^3, and only some heavy metals, such as gold, platinum, iridium, or osmium, have a higher density. Tungsten is also chemically very stable; it resists the effects of water or atmospheric conditions and reacts with oxygen only at higher temperatures. It is also a type 1 superconductor, i.e., its superconductivity is conditioned by a significant reduction in temperature (specifically for tungsten, it is 0.0154 K). This metal is rare on Earth and occurs in nature mainly in minerals such as wolframite, scheelite or stolzite. Its most common production is by metallurgy routes. The heavy ore fraction is mechanically separated, the concentrate is subsequently melted using NaOH and then leached in water, into which the formed sodium tungstate passes. By acidifying this solution, a tungsten oxide precipitate is separated. Pure tungsten is then produced by reducing tungsten oxide with hydrogen [16].

The use of this element is derived from its properties – primarily high density and melting temperature. A typical example is its use as a material to produce light bulb filaments with the operating temperature exceeding 1000 °C. Tungsten is also used as an electrode material for TIG (tungsten inert gas) welding, or in X-ray tubes, as its high electron density makes it ideal for generating bremsstrahlung. In alloys, tungsten primarily increases hardness and mechanical and thermal resistance, which is used, for example, in high-speed steels. The application of tungsten carbides in the production of machining tools is also essential. Most often, it is carried out with the admixture of cobalt by the method of powder metallurgy [16] [17].

The formation of surface coatings from pure tungsten or its carbides is considerably limited due to the high melting temperature. Currently, tungsten coatings are most often applied by PVD or CVD methods. These methods form coatings with thickness in a range of micrometers. However, for the prospective application in experimental fusion devices, a certain minimum critical coating thickness is considered, which would either be impossible or economically meaningless to deposit with the use of these methods. The solution here could be the use of thermal spray methods.

2.3 Thermal spray

In general, the deposition of surface coatings comprises a wide range of procedures, which in principle serve to modify and improve the properties of the functional surfaces of various components. Using this approach, for example, the core of the component can be made of a tough, lightweight material, while the protective coating ensures an increased hardness, abrasion resistance, or corrosion resistance of the surface. The coating deposition methods can be divided, among other criteria, according to the thickness of the applied layer. While technologies such as PVD and CVD apply coatings with thickness within the range of micrometers, thermal spray methods can create coatings with thickness exceeding units of millimeters, and in special cases, even more.

2.3.1 Principle of thermal spray methods

Thermal spray is a general term for technologies whose goal is to modify the base material by applying a relatively thick layer of metallic or non-metallic (e.g., ceramic) materials by the effect of melting the feedstock material. The pioneer of this technology can be considered the Swiss inventor Max Ulrich Schoop. In 1909 he patented a process in which lead powder was fed into an oxy-acetylene welding torch. The supplied powder subsequently melted and was carried by the flame stream of the burner onto a base material. Accelerated molten particles then gradually layered after contact with the base material to form a coating. This ground-breaking experiment can be considered the first execution of thermal spray, and it was soon followed by many technologies that are used to this day owing to their high deposition efficiency and low-cost operation [18].

As shown in Figure 6, thermal spray methods can be divided into two main groups according to the used type of the heat source, electrical and combustion.

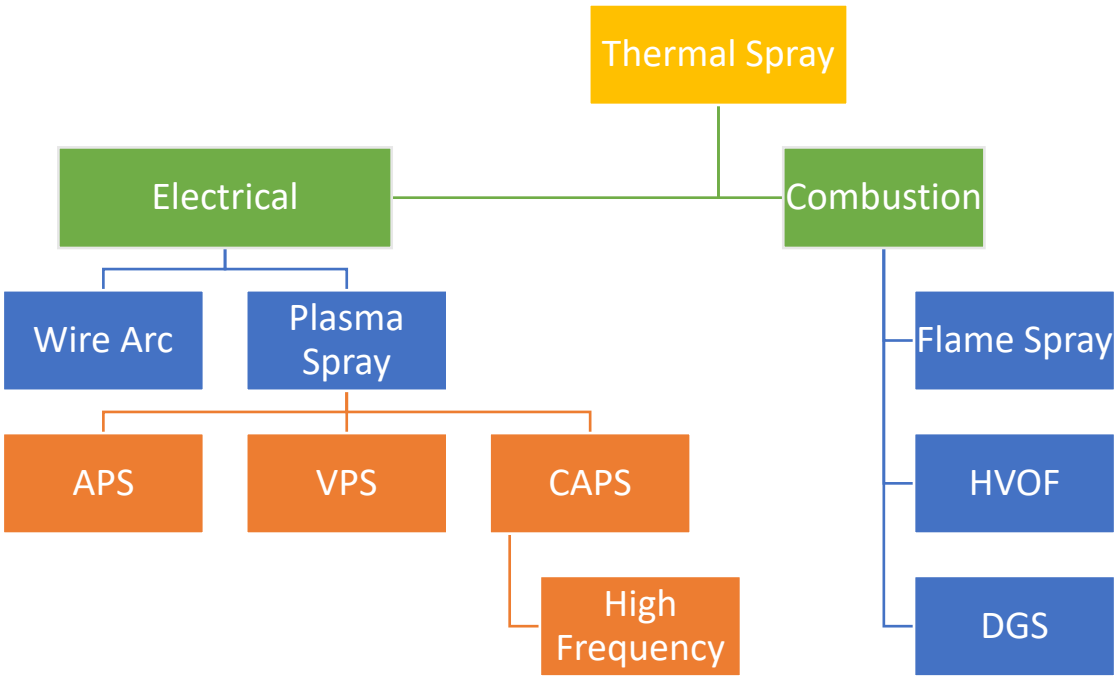

Figure 6: Classification of thermal spray technologies (modified from [19]).

A summary of thermal spray methods is described in the DIN EN 657 standard [20]. These technologies are described as a process in which additional material in the form of powder, rod or wire is supplied to a heat source, which melts it or converts it into a state of high plastic deformability. In this form, the material is subsequently accelerated by the stream of gases towards the surface of the component. Upon impact, the accelerated particles are deformed to form lamellar particles (so-called "splats") that adhere to the surface of the basic component and stack upon each other. Upon solidification, these splats form a heterogeneous lamellar structure further containing microcracks, unmelted particles, and inclusions such as oxidized particles of the sprayed metal. This type of microstructure is inherent to the thermal spray and is shown in Figure 7 [18] [21] [22].

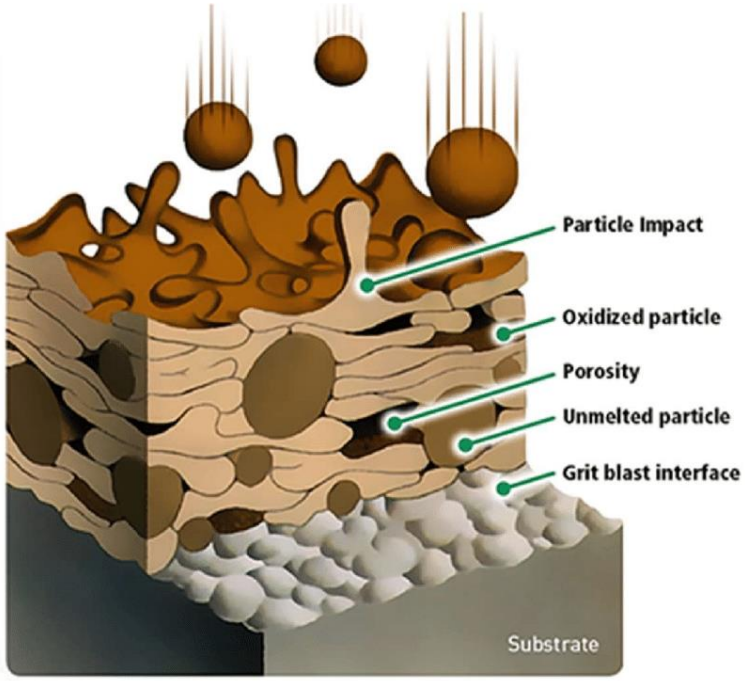

Figure 7: Typical microstructure of a thermal spray deposited coating [23].

The final structure of the coatings depends on the parameters of the application process. These, in turn, influence the in-flight temperature and speed of the molten particles, which are the most influential factors. At the same time, it is necessary to ensure the optimal distance of the application head from the base component; too small distance would not allow the molten particles to accelerate or melt sufficiently, and too large distance would result in a loss of speed of the particles or their partial in-flight solidification, which would negatively affect the resulting spray structure. Also, by choosing a suitable protective atmosphere, oxidation can be prevented, among other benefits [24].

For the planned application of tungsten, due to its high melting temperature, it is necessary to use a method with sufficient energy to ensure a proper melting and thus formation of a high-quality coating. Generally, thermal spray methods that use electricity as a heat source have higher operating temperatures. Especially technologies that work with plasma as the heat

source can reach tens of thousands of degrees Celsius. The following chapter will therefore be devoted to plasma deposition methods, as they are suitable candidates for depositing tungsten protective coatings for the internal components of fusion reactors.

2.3.2 Plasma spray

Plasma, also the fourth state of matter, is an ensemble of charged and neutral particles in various quantum states with a space charge of approximately zero. This state is also known as quasi-neutrality. Plasma is divided into isothermal and non-isothermal based on the energy delivery method. In the case of plasma deposition technology, non-isothermal plasma is used, which is characterized by a higher temperature of electrons than other contained particles. At the same time, this type of plasma does not spontaneously exist in nature and must therefore be maintained artificially. Devices used for plasma application can generate plasma either by electric arc or radio frequency electromagnetic field (so-called inductively coupled plasma) [25]. The following two sections will be devoted to both types of the plasma spray methods, as they are, due to their nature, one of the possible solutions to produce protective coatings for the internal structures of fusion reactors.

DC plasma spray

DC plasma spray is a very universal method that is suitable for creating protective coatings with high quality and unique properties. This technology consists of melting the additional material in the form of powder, rod or wire using a plasma stream generated by a DC electric arc. This arc is positioned between two electrodes, a cathode usually made of thoriated tungsten and anode made of copper. Plasma forming gas, most often argon, flows between them, and is subsequently ionized by the DC electric arc to form a high-temperature plasma. The added material is fed by carrier gas into the plasma stream, melted, and the molten particles are carried away at speeds of 180 to 300 m/s towards the surface of the component [25].

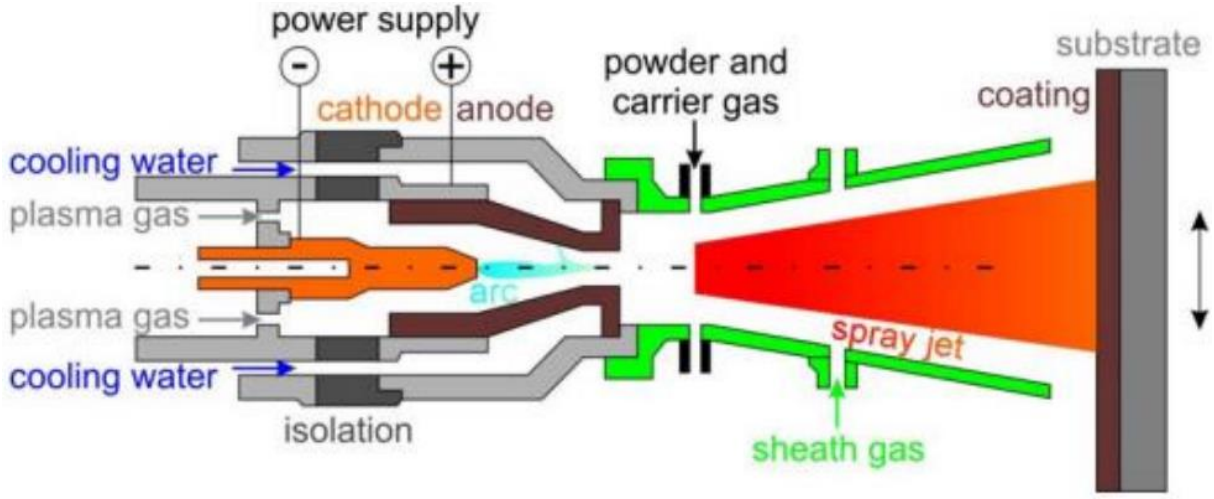

Figure 8: DC plasma spray method [21].

Due to the temperature of the plasma, which can reach up to 30,000 degrees Celsius when using the electric arc generation, the environment may be strongly oxidizing when

performed in air. This can have a negative effect on the resulting structure and mechanical properties of the coating and the formation of oxide inclusions is therefore undesirable in most cases. However, oxidation can be prevented by working in controlled atmosphere. Such methods are referred to as CAPS (controlled atmosphere plasma spray) or VPS (vacuum plasma spray).

RF-ICP

Inductively-coupled plasma technology works on a slightly different principle than the DC plasma generation. First and foremost, no arc is needed. In fact, the technology does not even use electrodes. Instead, the gas flow (most often argon) is ionized by an electromagnetic field formed by a copper induction coil wired around a ceramic tube inside the plasma torch, as shown in Figure 9. The plasma torch must be intensively cooled, most often with water. The source of the high-frequency current in the coil is a radio frequency generator, and this current then generates an oscillating electromagnetic field. The plasma generation then begins by the ignition of the gas, which is ensured by a spark plug. After the ignition, free electrons are formed inside the plasma torch and accelerated using the created electromagnetic field. These free electrons then collide with gas atoms, thereby transferring part of their kinetic energy. Consequently, the gas atoms are heated to the ionization temperature and a chain reaction that generates the inductively-coupled plasma is created. Plasma generated by this method can reach temperatures of up to 10,000 °C (i.e., significantly lower than plasma generated by an electric arc), with the commonly used temperature range from 5,000 to 7,000 °C [21] [26].

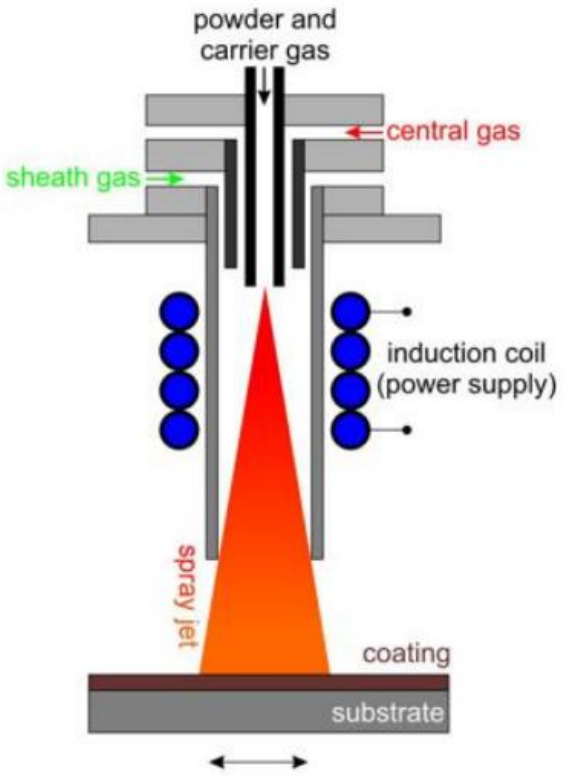

Figure 9: RF-ICP spray method [21].

Deposition of the coatings by this method is similar to deposition using plasma generated by an electric arc. In contrast to the plasma generated by an electric arc, in RF-ICP, the in-flight speeds of the particles are significantly lower, only around 30 m/s, which causes visible differences in the microstructure of the coatings. These differences mainly consist of a higher content of pores in the coatings prepared by the RF-ICP method [21] [24]. A significant advantage of the RF-ICP is that the deposition takes place in a controlled atmosphere, which ensures protection against the oxidation or other undesired reactions of the coating material [27].

In this thesis, the procedure of using the RF-ICP method for the optimization of tungsten coatings on steel substrates for potential fusion applications will be described in detail. The coatings will then be analyzed to observe the influence of the selected deposition parameters on the quality of the coatings.

3 Experimental

This section will describe the experimental details of the RF-ICP deposition of W coatings on steel substrates. Two different tungsten powders were used, and the deposition matrix consisted of 12 runs, comprehending the influences of four different spray parameters.

3.1 Used materials

3.1.1 Powders

Two different tungsten powders denoted as P1 and P2 were used as a feedstock material for the deposition to observe a possible influence of the particle sizes and shape. As shown in Figure 10, powder P1 consisted mainly of spherical particles as a result of its spheroidization production route and its purity was 99.9%. The particle size distribution of the powder P1 measured by laser scattering (Mastersizer 3000 device, Malvern Panalytical, UK) is shown in Figure 12. The 10% and 90% volumetric particle size quantiles were determined as 16 µm and 49 µm, with the average particle size being approximately 29 µm.

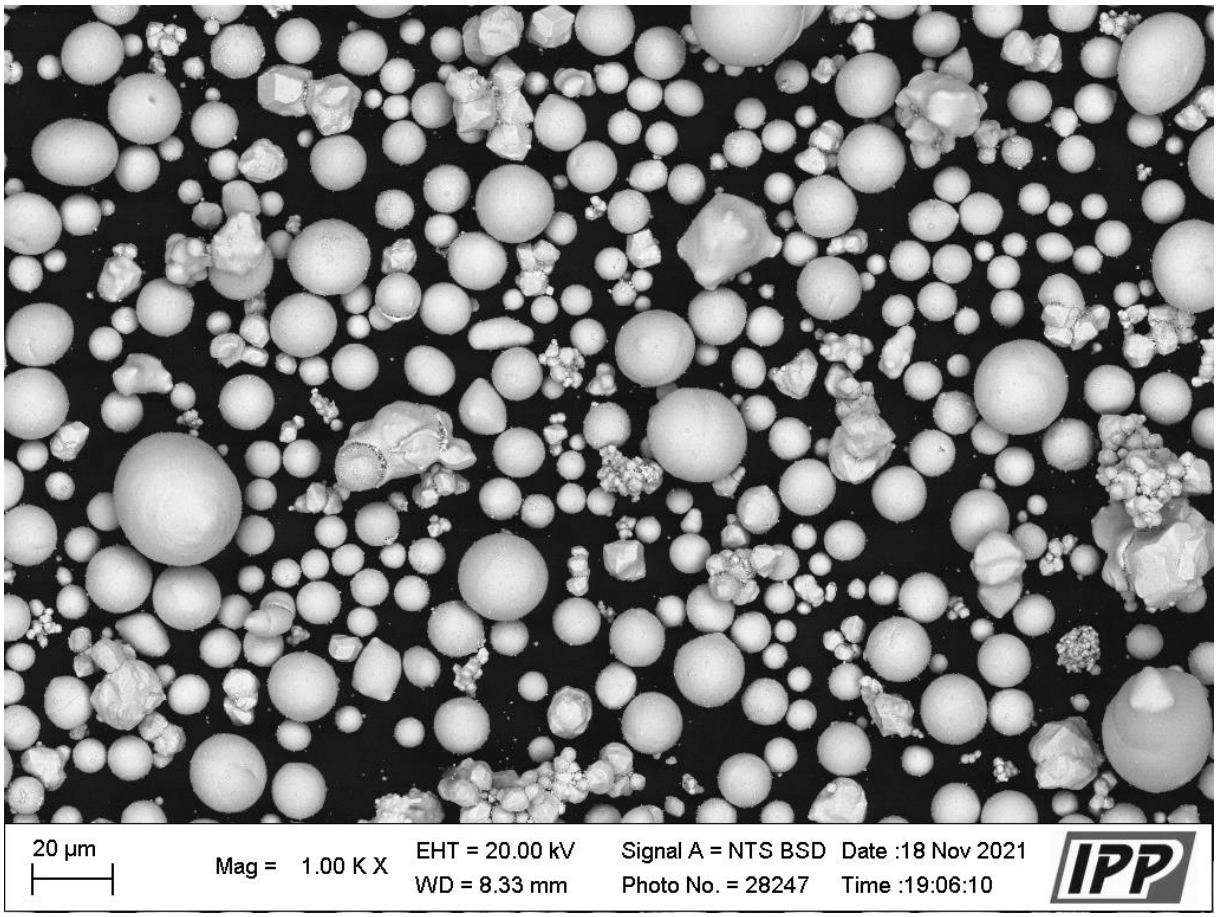

Figure 10: Morphology of the P1 powder particles.

The morphology of the powder P2 with purity over 99.5% is shown in Figure 11. As opposed to the spherical character of P1, P2 particles exhibited an angular character. Again, this was a consequence of the production process, hydrogen reduction of tungsten ores (as described in Chapter 2.2). Particle size distribution for powder P2 can be seen on Figure 12. The

10% and 90% particle size quantiles were determined as 11 and 36 µm with the average particle size being approximately 20 µm. This measurement was again carried out by laser scattering. The seeming discrepancy of the measured values with the particles shown in Figure 11 is given by the tendency of the powder particles to agglomerate into clusters.

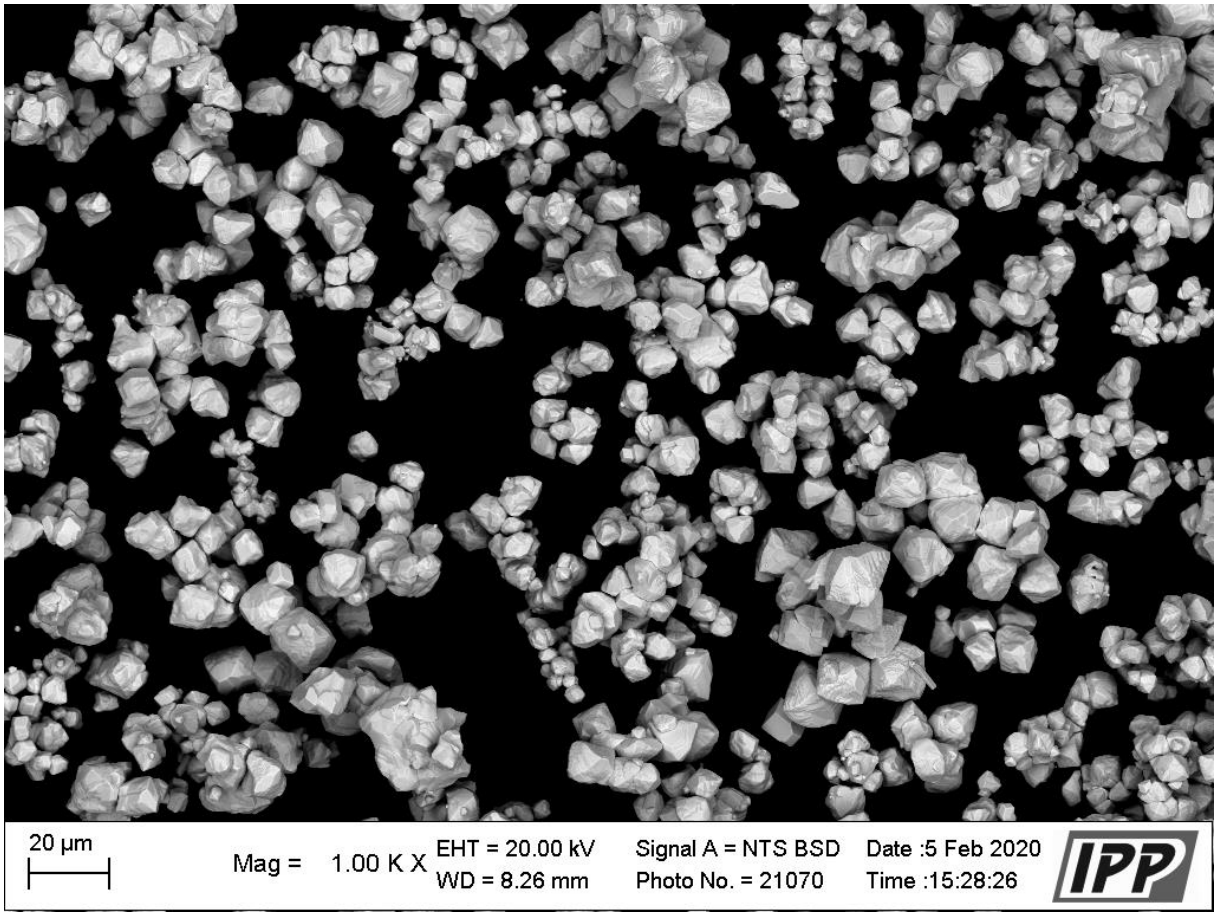

Figure 11: Morphology of the P2 powder particles.

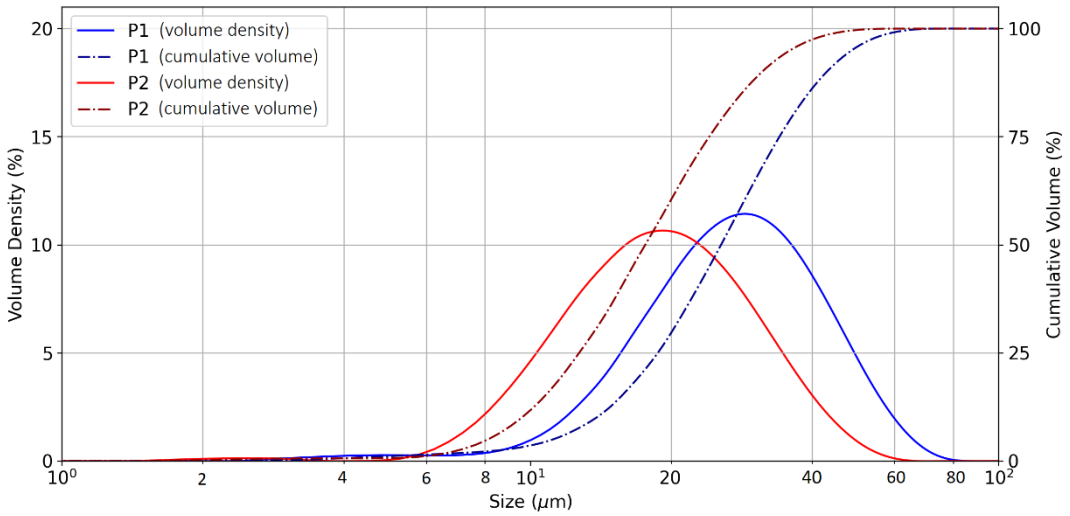

Figure 12: Volumetric particle size distribution of the used powders.

3.1.2 Substrates

The substrates were made of AISI 304 stainless steel, which is used as a replacement of the actual PFC steel (Eurofer) as it has similar properties (mainly thermal conductivity) and the use of Eurofer steel would not be economical for the purpose of optimization of the deposition process. All substrates were cut to samples of 60 × 20 × 3 mm^3, which are dimensions required for the sample holder used in the RF-ICP device. Figure 13 shows the geometry and appearance of the used substrates.

Prior to the deposition, the substrates were grit blasted to break the surface oxide layer and roughen their surfaces, thereby increasing the adhesion of the coating. The grit blasting was done using 100–300 µm corundum particles at an air pressure of 0.6 MPa from a distance of approximately 150 mm under almost 90°. The grit blasting distance and angle are important process parameters as they affect surface roughness and content of residual corundum particles [28]. The grit-blasted substrates were then immersed in acetone and placed in an ultrasonic cleaner for 10 minutes. The ultrasonic procedure is commonly used to reduce the occurrence of residual grit particles as these can negatively affect the coating adherence.

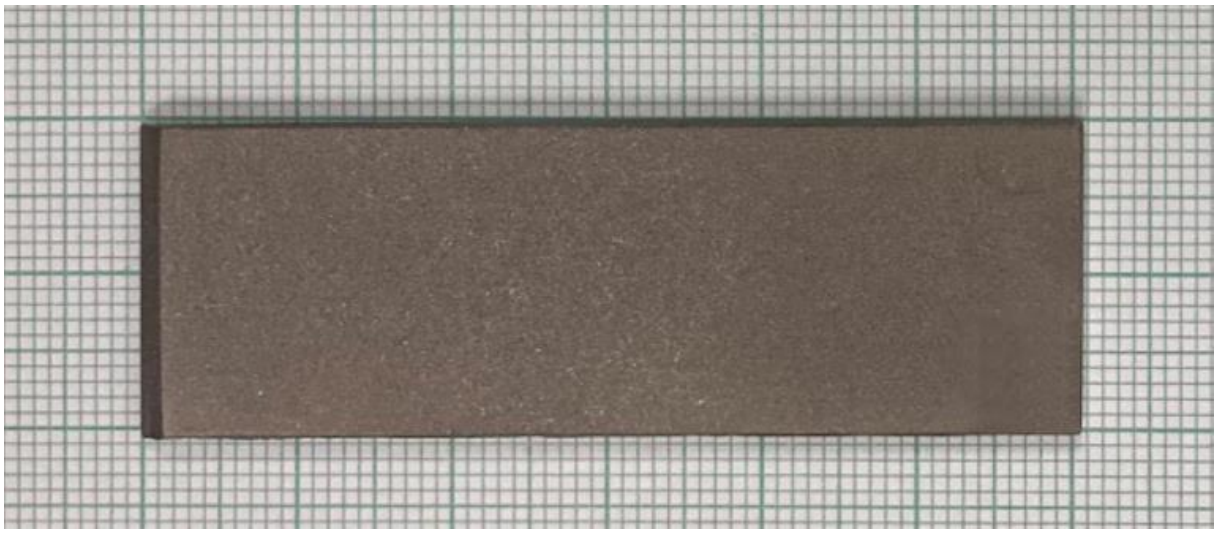

Figure 13: AISI 304 steel grit blasted substrate used for the experiment.

3.2 Coating deposition process

3.2.1 RF-ICP deposition device

Tekspray 15 (see Figure 14) device by Canadian manufacturer Tekna with a maximum power output of 15 kW was used for the deposition. This device operates in a protective atmosphere, and it is primarily used for research and development. According to the manufacturer, this device stands out by depositing coatings with high density and excellent structural characteristics.

Figure 14: Tekna Tekspray 15 device.

To remove any parasitic electromagnetic fields and protect the operator from the high-frequency radiation, the device is designed as a Faraday cage. It consists of two main parts - the control panel and gas flow meters, and an inner chamber, shown in Figure 15. The control panel is used to set the process parameters, and the gas flow meters allow control of the gases used in the process, in our case argon and hydrogen. The volume flow rate of gases is given in units of slpm, which define the volume of gas flow per unit of time at a temperature of 0 °C and an atmospheric pressure of 100 kPa. Argon is typically used as the main plasma-forming gas, but also as a carrier gas, while the design of the device allows the addition of, e.g., hydrogen or helium to increase the enthalpy and thereby increase the efficiency of the process [29].

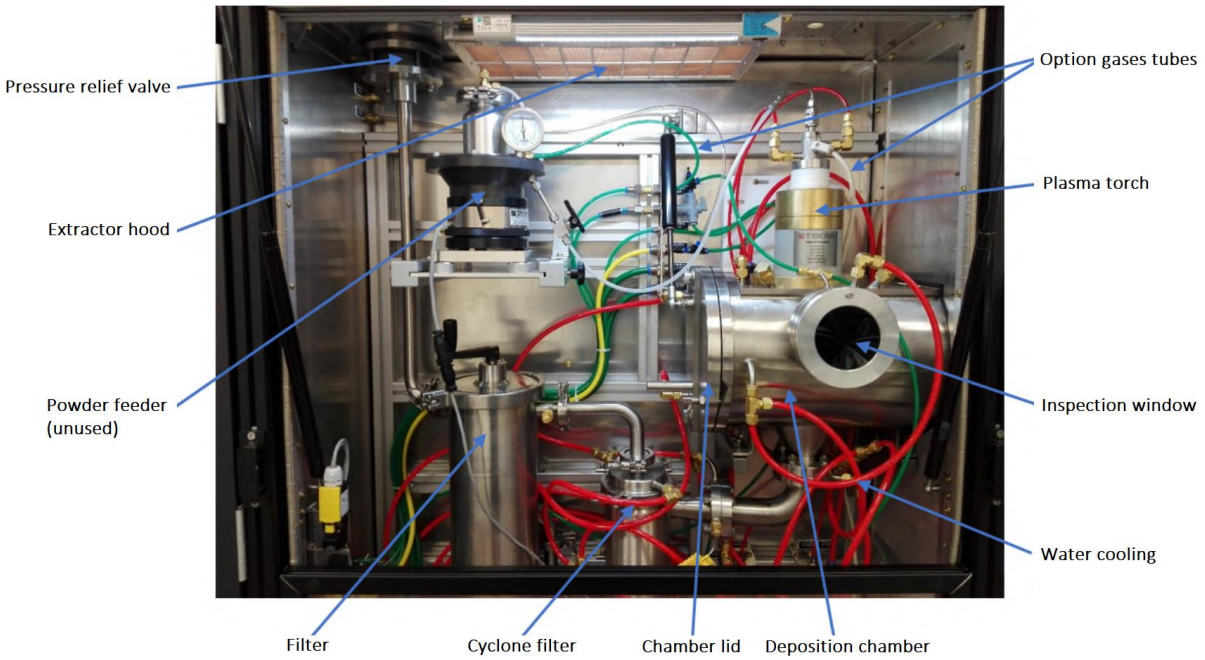

Figure 15: Detailed view of inside components of Tekspray 15 (modified from [30]).

Tekspray 15 uses additional material in the form of powder for the deposition of the coatings. The original powder feeder supplied with the device was replaced by an external feeder Twin-system 10-2 disk feeder (Plasma-Technik, Switzerland) for more reliable delivery of the powder into the deposition chamber. In the external feeder, the feed rate can be finely adjusted, and a steady, fluctuation-free delivery can be ensured.

The plasma generation takes place inside a water-cooled plasma torch (Figure 16). This torch is attached to a double-walled cylindrical deposition chamber made of stainless steel. Access to the deposition chamber is ensured by a sealed lid, and the spraying process itself can be monitored through a small inspection window.

Figure 16: TekSpray 15 plasma torch.

Inside the deposition chamber, the substrates are mounted on a hexagonal sample holder placed at the end of a rotating shaft, as shown in Figure 17. This rotating, water cooled shaft was installed as part of the own modifications, as the original shaft was designed for

application on a single graphite substrate of circular shape only. However, spraying onto graphite substrates is not relevant for fusion applications, and water cooling of the new shaft enables the deposition of coatings on materials with lower melting temperatures. This is important for our experiment, where coatings are deposited onto AISI 304 steel substrates. The new shaft supports, among other things, a linear movement under the torch without revolving in case of deposition on one sample, or a combination of linear movement and revolution around its axis, which opens up the possibility of evenly spraying onto up to six samples at the same time.

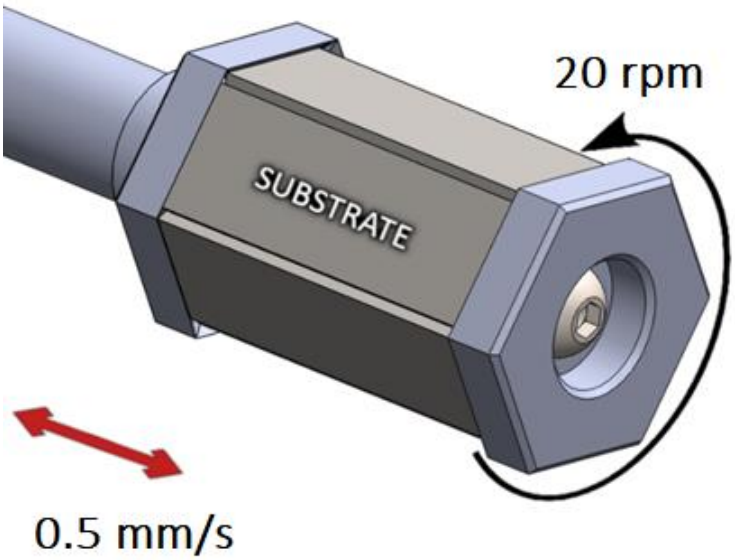

Figure 17: New water-cooled shaft with hexagonal sample holder.

3.2.2 Deposition process and characterization of the coatings

The experimental part of this work consisted in investigating the influence of four selected deposition parameters on the quality of the coatings: powder feed rate, feedstock powder properties (particle shape and size), and the type and amount of the carrier gas used.

Table 1 shows the individual parameters for the twelve tested combinations denoted as RF1–12. For samples RF1–6, powder P1 was used as a feedstock material. For samples RF7–12, powder P2 was used. The corresponding feed rates are slightly different for both powders, as the powder feeder does not allow to control exact amount of the supplied powder. Instead, the speed of the rotary disc of the powder feeder can be adjusted, giving slightly different feed rate for the two dissimilar powders. The exact feed rates of the supplied powders (in grams per minute) were measured by an additional experiment.

Table 1: Deposition parameters for samples RF1-RF12.

<table>
<tr><th rowspan="2">Sample</th><th rowspan="2">Powder</th><th rowspan="2">Powder feed rate (g/min)</th><th colspan="3">Gas flow volume (slpm)</th></tr>
<tr><th>Sheath gas</th><th>Central gas</th><th>Carrier gas</th></tr>
<tr><td>RF1</td><td rowspan="6">P1</td><td>3.2</td><td rowspan="12">Ar 35
+
He 3.4</td><td rowspan="12">Ar 10</td><td rowspan="2">Ar 8</td></tr>
<tr><td>RF2</td><td>1.6</td></tr>
<tr><td>RF3</td><td>3.2</td><td rowspan="2">Ar 6</td></tr>
<tr><td>RF4</td><td>1.6</td></tr>
<tr><td>RF5</td><td>3.2</td><td rowspan="2">He 8</td></tr>
<tr><td>RF6</td><td>1.6</td></tr>
<tr><td>RF7</td><td rowspan="6">P2</td><td>3</td><td rowspan="2">Ar 8</td></tr>
<tr><td>RF8</td><td>1.5</td></tr>
<tr><td>RF9</td><td>3</td><td rowspan="2">Ar 6</td></tr>
<tr><td>RF10</td><td>1.5</td></tr>
<tr><td>RF11</td><td>3</td><td rowspan="2">He 8</td></tr>
<tr><td>RF12</td><td>1.5</td></tr>
</table>

The first step of each deposition was preheating the substrates. The shaft moved at a speed of 0.5 mm/s under the plasma torch in the direction visualized in Figure 17 by the red arrow for 80 seconds, while revolving at 20 rpm around the axis perpendicular to the spray direction to evenly heat all six substrates. During the preheating, the powder feeding was turned off. Preheating is a commonly used procedure that positively affects, e.g., the adhesion of the deposited layers [26]. The shaft then returned to its starting position, while powder began to be fed into the deposition chamber, which was visually manifested by a color change of the plasma. After a short stabilization period, the deposition began.

For the deposition, the torch power was set to a maximum value, which is 15 kW. Using lower power of the plasma torch was not considered, as previous studies have shown rather

poor results for the deposition of tungsten [31] [32]. The substrates were placed below the plasma torch at a stand-off distance of 70 mm and revolved at 20 rpm while maintaining a linear shaft speed of 0.5 mm/s. The total spraying time was 640 s for every sample (8 passes under the torch, each pass took 80 s). The chamber pressure was kept at 103.4 kPa for all samples. The flow rate of the sheath gas was 35 slpm of argon with addition of 3.4 slpm of hydrogen; the central gas flow rate was 10 slpm of argon for all samples. The influence of using different carrier gases (argon and helium) and its flow rates (6 and 8 slpm for Ar, 8 slpm for He) was observed. After the deposition was complete, the samples were left to cool to a room temperature in the protective atmosphere.

3.2.3 Characterization of the coatings

The obtained samples were cut using a high-speed saw, mounted in epoxy and prepared according to a standard metallographic procedure. The samples were ground using SiC emery papers of FEPA 1200, 2000 and 4000 grit size (the total grinding time was 4 min and 40 s), followed by polishing using 1 µm polycrystalline diamond suspension for 10 min using Tegramin-25 device (Struers, Denmark). As the last step, the samples were oxide-polished for 2 min using 0.04 µm colloidal silica suspension solution. Evaluation of the prepared cross-sections was then performed using EVO MA 15 scanning electron microscope (Zeiss, Germany). The porosity of the coatings was then evaluated using image analysis using the freely available ImageJ software. The porosity was determined from the average of three measurements.

4 Results and discussion

In this chapter, the properties of the twelve W coatings prepared by the RF-ICP technology will be presented, and the influence of the four selected deposition parameters will be discussed.

4.1 Results overview

In the first phase of the experimental part, a total of six samples were coated with the use of powder P1. For sample RF1, argon was used as a carrier gas with a flow rate of 8 slpm. In accordance with the know-how obtained with similar powders, the deposition was carried out with the maximum power of the system, 15 kW [31] [32]. The feed rate of the powder was 3.2 g/min. Other process parameters can be seen in Table 1. As shown in Figure 18, the coating had a uniform thickness of approximately 1050 µm. There was a relatively frequent occurrence of individual, not very well connected unmelted particles in the coating. This is typically connected to increased porosity levels, measured as 41.4% in this case. Dendritic microstructure inside some splats was present near the mutual interface with the substrate and gradually disappeared with increasing thickness. The smaller powder particles appeared to form regular, well flattened splats. Contrary to this, the bigger particles seemed to be melted only partially, as they preserved their original spherical shape, regardless of the position in the coating. Local delamination of the coating from the substrate could be observed on the mutual interface.

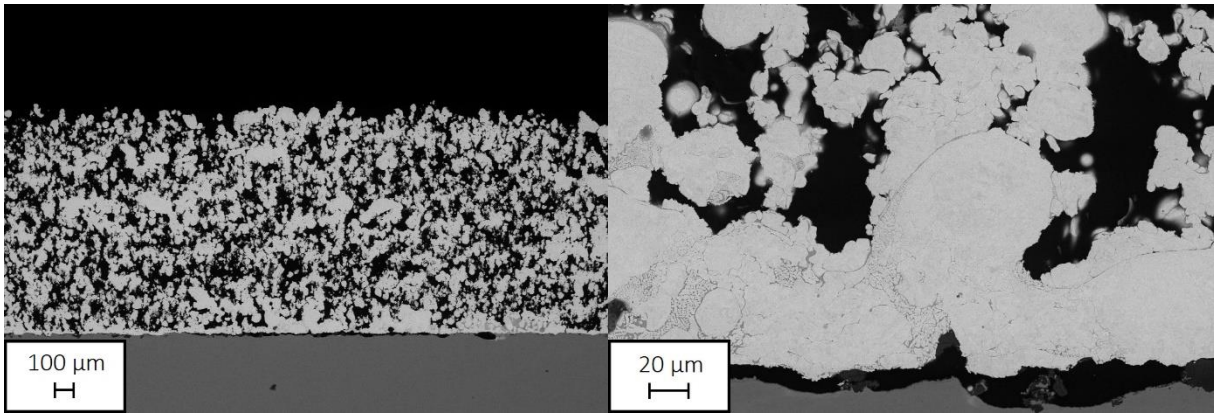

Figure 18: Microstructure of the RF1 coating.

After the evaluation of the sample RF1, it was suggested to reduce the powder feed rate to ensure proper melting of the individual (especially the bigger) particles as the total plasma enthalpy would be distributed into fewer particles. The feed rate was therefore halved (1.6 g/min), while the other process parameters were maintained identical to those of RF1, as shown in Table 1.

As shown in Figure 19, the sample RF2 showed a coating with a thickness reaching up to 360 µm. As with RF1, a significant number of unmelted particles was still present. However, an occasional presence of lamellar, dendritic structure consisting of small, mutually connected splats was observed close to the mutual interface. With the increasing distance from the

interface toward the free surface, the particles appeared to preserve their original spherical shape, which suggested their insufficient melting in the process. In comparison with RF1, a slightly lower porosity was measured for this sample (34.2%). An occasional delamination of the coating was observed on the mutual interface.

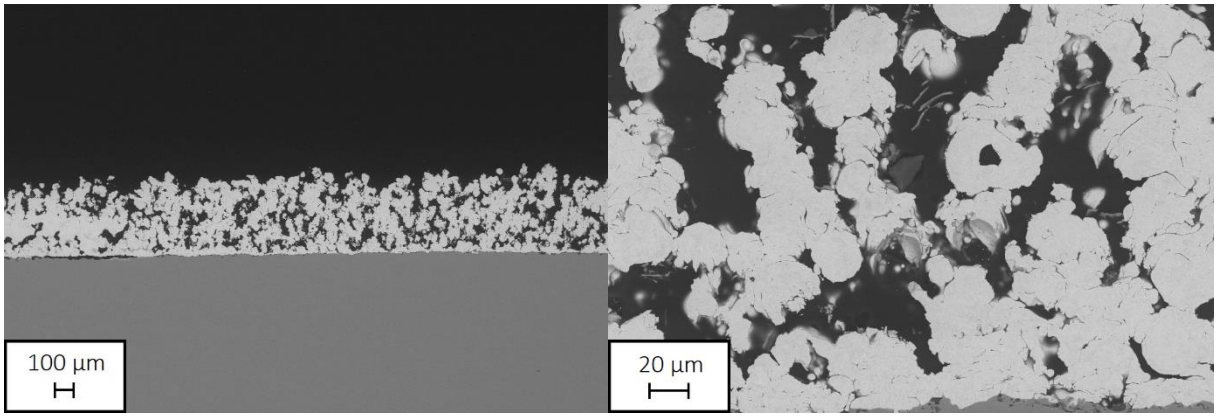

Figure 19: Microstructure of the RF2 coating.

It was decided for the following deposition to reduce the flow rate of carrier gas, as the carrier gas drains enthalpy of the plasma, thereby reducing the heat intake of the powder particles.

For the sample RF3, the argon carrier gas flow rate was reduced to 6 slpm. The powder feed rate was set back to 3.2 g/min (its halved value was later tested as well, RF4). Other parameters are shown in Table 1. The coating showed a thickness of approximately 925 µm, as shown in Figure 20. In comparison with RF1 (same powder feed rate, but higher Ar carrier gas flow rate), RF3 exhibited better microstructure, as the number of unmelted, poorly connected particles partially decreased. The better melting of the particles also resulted in a decreased porosity (32.3%). A lamellar structure was observable locally, as was a higher number of well-merged splats, especially near the mutual interface.

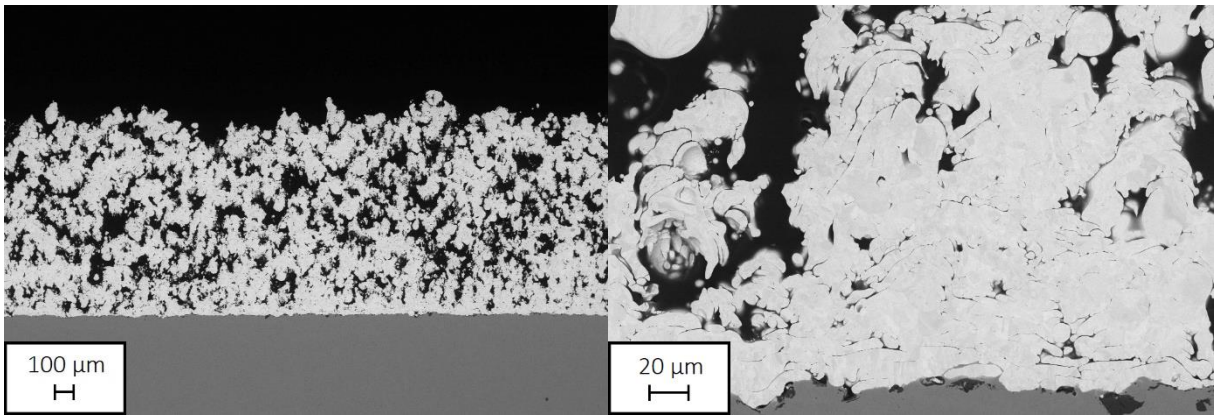

Figure 20: Microstructure of the RF3 coating.

To follow the plan, the sample RF4 was deposited with the use of reduced-flow argon as a carrier gas (6 slpm) and a halved powder feed rate (1.6 g/min) to possibly observe any potential synergy of the two factors. Other process parameters are shown in Table 1. As shown

in Figure 21, the thickness of the coating was irregular, reaching up to 380 µm. However, the coating RF4 exhibited the best microstructure so far. There were almost no unmelted particles present, which resulted in a lowered porosity (16.7%) in comparison with the previous three samples. The dendritic microstructure was present on the coating-substrate interface, where the splats appeared to be lamellar and well merged. A diffusion of the substrate into the coating was observed near the mutual interface as well as local signs of delamination of the coating. With increasing distance from the interface, the splats made of bigger particles appeared to gradually lose their lamellar shape and became elliptical or even spherical, especially near the free surface of the coating.

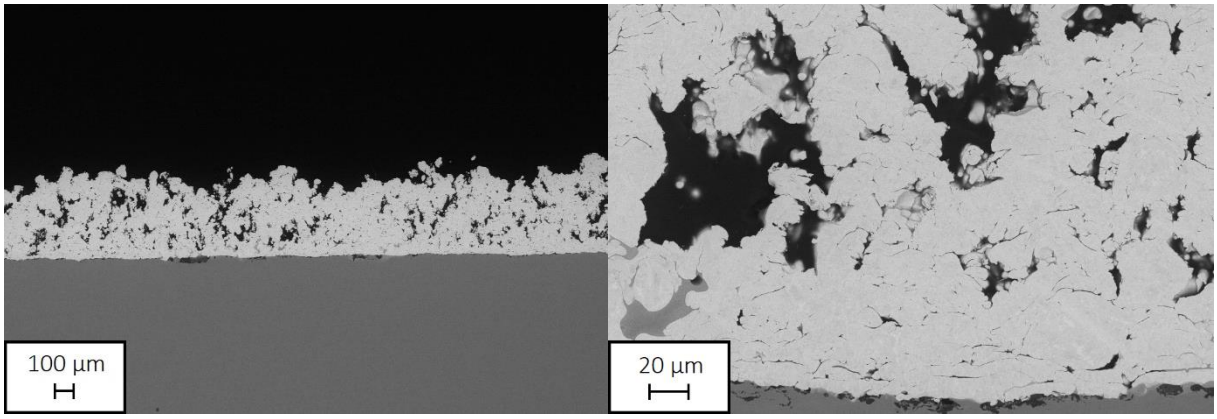

Figure 21: Microstructure of the RF4 coating.

To further lower the cooling effect of the carrier gas and provide enhanced heat transfer to the particles, a further reduction of the Ar flow was considered. Unfortunately, upon experimental trials, it was found that the Ar flow rates below 6 slpm cannot be used as the carrier gas then loses its ability to hoist the powder particles from the powder feeder and carry them into the process. Therefore, as the next adjustment, the use of He as carrier gas instead of Ar was suggested, as the use of this gas can substantially increase the enthalpy of the plasma and therefore improve the thermal transfer to the particles. The use of He as a carrier gas was possible due to the external modification of the system, which regulates the flow rate to be 8 slpm. RF5 was therefore deposited with the use of He as a carrier gas with a flow rate of 8 slpm. To allow a direct comparison with RF1 (8 slpm of Ar), all other spraying parameters were preserved, as shown in Table 1.

The sample RF5 showed very promising results toward optimization of the parameters. The thickness was uniform and ranged up to 780 µm (730 µm when excluding the delamination), as shown in Figure 22. The entire coating exhibited a compact, lamellar microstructure and the individual splats of typical sizes >20 µm adhered well. A small amount of porosity (10.8%) was still observed as well as a negligible occurrence of bigger pores and unmelted particles. A continuous delamination appeared close to the coating-substrate interface (not considered in the porosity measurement).

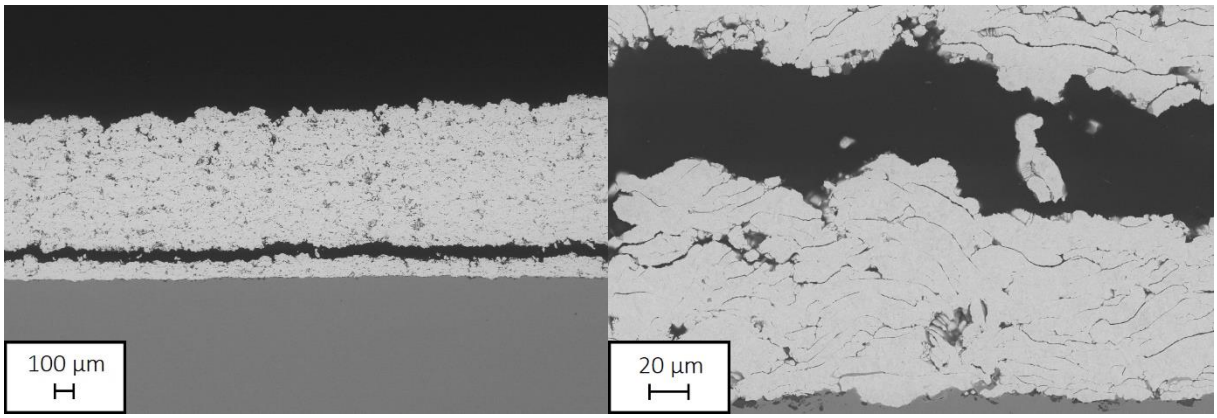

Figure 22: Microstructure of the RF5 coating.

To complete the matrix for the P1 powder, sample RF6 was deposited with the use of helium as a carrier gas with a flow rate of 8 slpm, and a reduced powder feed rate set to 1.6 g/min (Table 1). The coating had an uniform thickness of approximately 325 µm, as seen in Figure 23. The dense lamellar structure of the RF6 coating consisted mainly of well-merged splats within the entire coating. The coating showed a negligible amount of intersplat porosity and no occurrence of unmelted particles. The porosity was measured to be the lowest among the first six samples, 7.4%. No signs of delamination on the interface coating-substrate were observed as well.

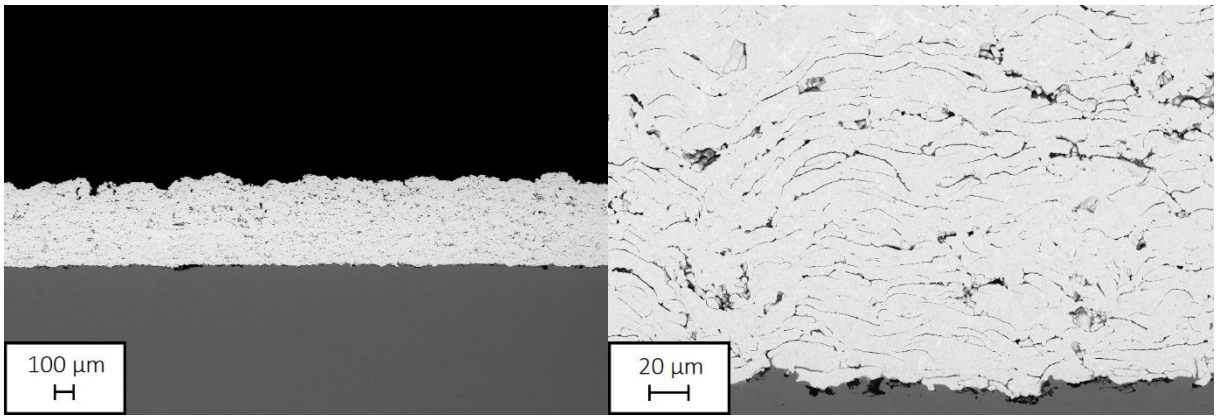

Figure 23: Microstructure of the RF6 coating.

In thermal spraying, the quality and characteristics of the feedstock powder is of utmost importance, one of the critical parameters influencing the final coating quality. To investigate the potential of further optimization of the coatings, the six depositions (RF1-RF6) were repeated with the use of another tungsten powder.

The second used powder, denoted as P2, had slightly smaller, polyhedron-shaped particles that exhibited a tendency to agglomerate into somewhat bigger clusters. In comparison with P1 powder, this powder also had a narrower particle size distribution. This

means that powder P2 contained a lower number of large particles (>80 µm), that are more difficult to completely melt using the 15-kW system.

Sample RF7 (an equivalent of RF1) was deposited with the use of Ar as a carrier gas with a flow rate of 8 slpm, the feed rate was set to 3 g/min (the reason of the slightly different feed rate to powder P1 is given by the feeding mechanism, as explained in section 3.2.2). The other process parameters are provided in Table 1. As with the P1 powder, the coating RF7 showed a thickness ranging up to 375 µm, as shown in Figure 24. A rather high porosity was observable (23%), as well some unmelted, poorly connected particles. In certain parts of the coating (especially close to the mutual interface), lamellar microstructure with occasional occurrence of well-adhered splats was observed. Closer to the substrate-coating interface, the splats were properly flattened, while with an increasing distance toward the free surface, they appeared to be less deformed in the process.

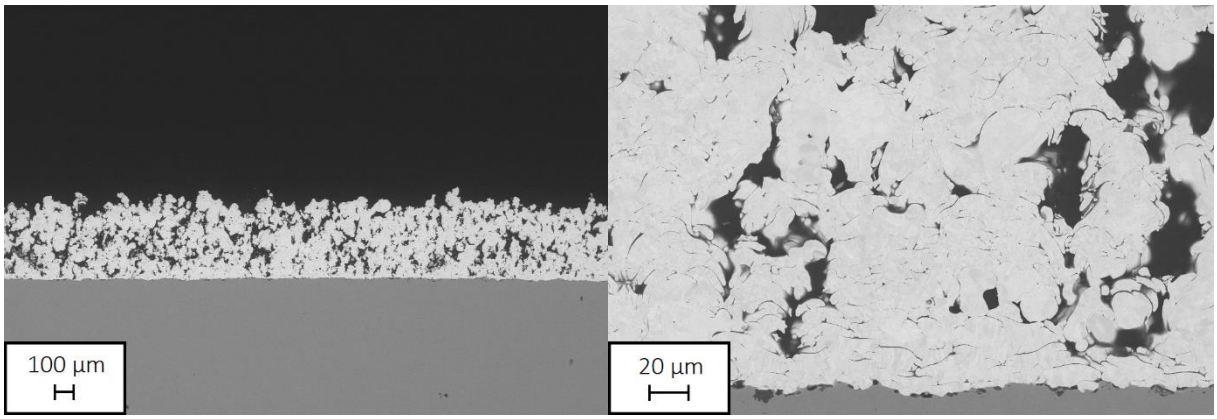

Figure 24: Microstructure of the RF7 coating.

The coating RF8 was deposited with the use of Ar as a carrier gas with a flow rate of 8 slpm, but the feed rate reduced to 1.5 g/min (Table 1). The coating showed an uneven thickness ranging up to 150 µm, as shown in Figure 25. In comparison with RF7, halving the feed rate appeared as a remarkable improvement in the microstructure, as the splats appear to be mostly connected throughout the entire cross-section. The splats formed a lamellar structure near the mutual interface, and with increasing distance toward the free surface, they lose their lamellar shape and appeared poorly deformed. There was almost no occurrence of unmelted particles, especially in the lower part of the coating. There were no signs of delamination of the coating as well. A rather low porosity was recorded for RF8 (10.8%).

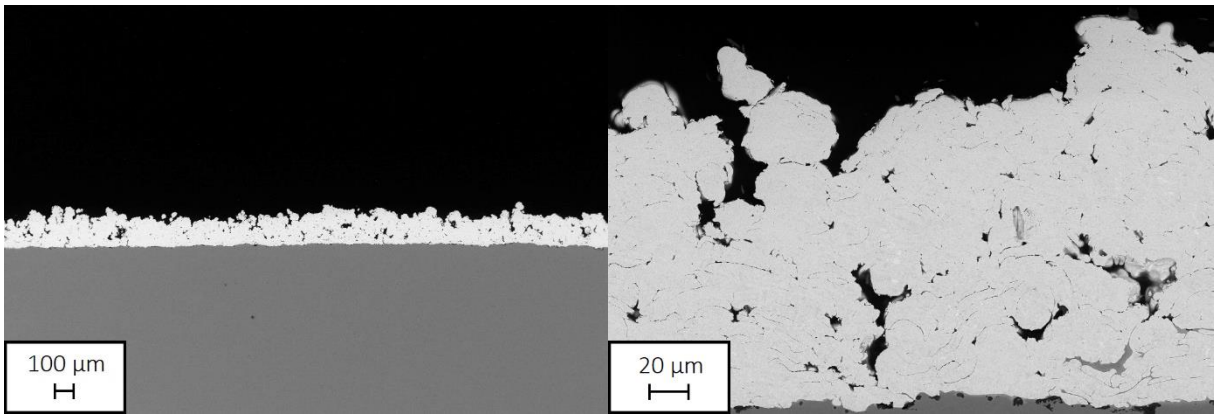

Figure 25: Microstructure of the RF8 coating.

Sample RF9 was coated with the use of reduced flow of Ar as a carrier gas (6 slpm) and the feed rate of 3 g/min (Table 1). As seen in Figure 26, the coating RF9 showed a thickness reaching up to 405 µm. The lower part of the coating showed a dense, lamellar microstructure with almost no unmelted particles. Well-deformed and merged splats were observed in this part of the coating, and toward the free surface, less flattened splats were present, which led to a slightly increased porosity in the upper part of the coating. No signs of delamination were present at the interface coating-substrate. A rather low porosity (10.2%) was recorded for RF9.

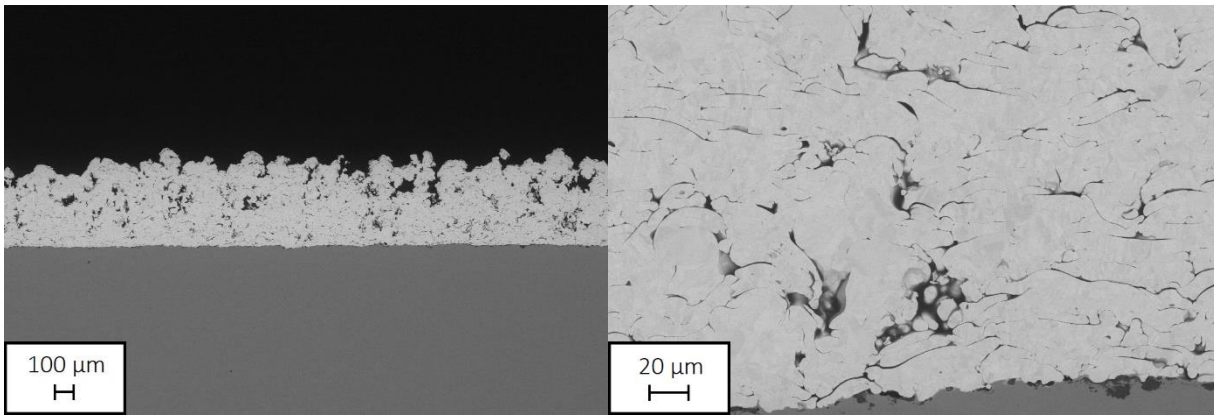

Figure 26: Microstructure of the RF9 coating.

The coating RF10 was deposited with the use of argon as a carrier gas with a flow rate of 6 slpm, and the feed rate reduced to 1.5 g/min (Table 1). As seen in Figure 27, a high-quality coating has been achieved with a thickness approximately 130 µm. A compact lamellar structure consisting purely of well merged flattened splats was observed throughout the whole coating. In this case, the interface of the individual splats could have been barely distinguished. The coating-substrate interface also showed no signs of delamination. For RF9, the porosity was measured to be very low, 4.8%.

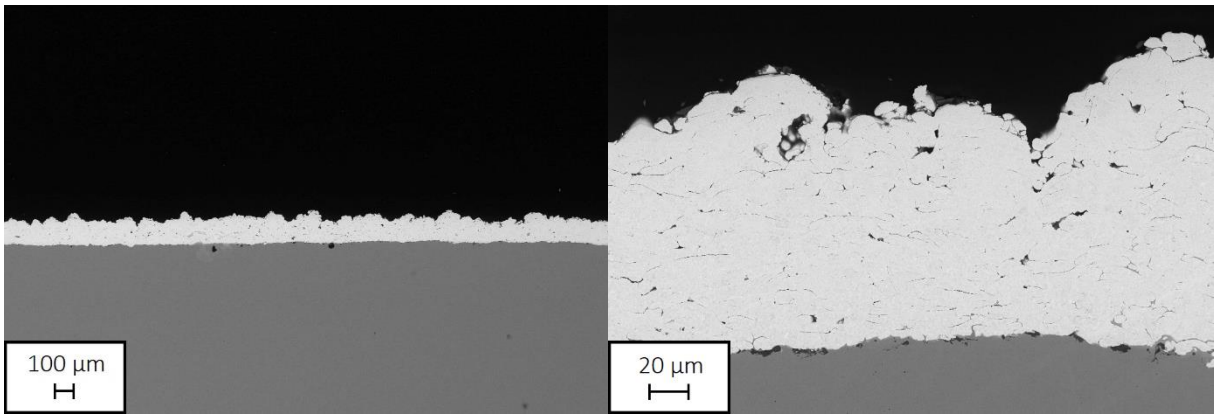

Figure 27: Microstructure of the RF10 coating.

To complete the full experimental matrix, two last samples prepared using the P2 powder were sprayed with helium at 8 slpm as the carrier gas. The coating RF11 was prepared with the powder feed rate set to 3 g/min (Table 1). Again, a high-quality coating has been achieved, shown in Figure 28. The coating had a uniform thickness of approximately 215 µm. Almost no unmelted particles were present, as well as no signs of delamination of the coating. The splats of typical sizes >20 µm exhibited consistent lamellar shape within the whole coating and their mutual interface could have been barely distinguished, which resulted in low porosity (7%).

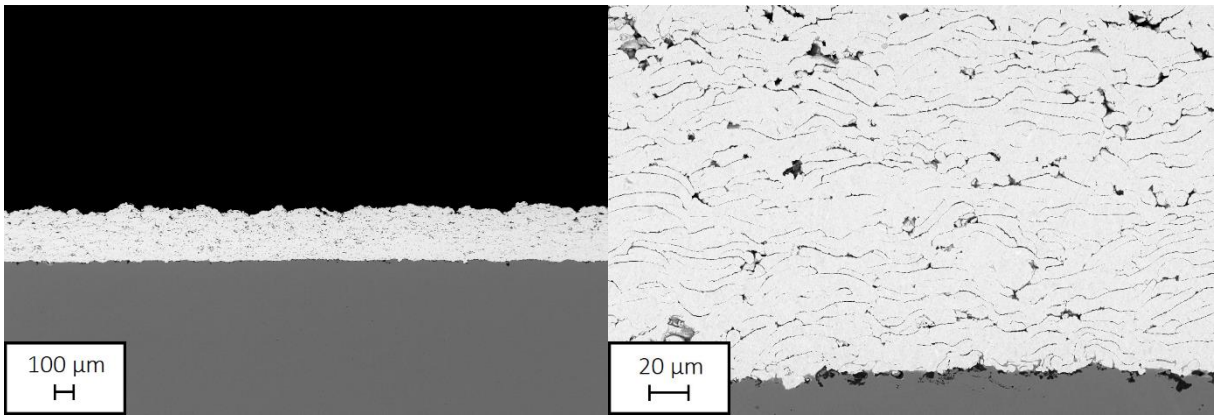

Figure 28: Microstructure of the RF11 coating.

The last deposition RF12 was done with the use of helium as a carrier gas with a flow rate of 8 slpm and the feed rate reduced to 1.5 g/min (Table 1). As with RF11, a high-quality coating has been achieved, as shown in Figure 29. The coating exhibited a thickness reaching 110 µm without any signs of delamination of the coating. A lamellar microstructure comprising mostly of well-merged splats was observed, especially near the interface coating-substrate with no signs of delamination. The substrate appeared to be partially locally melted, while the surface of the coating showed condensates of evaporated powder particles. This resulted in slightly increased porosity in the upper part of the coating. For this last sample, the average porosity was measured to be 7% (the more porous top regions were excluded from the measurement).

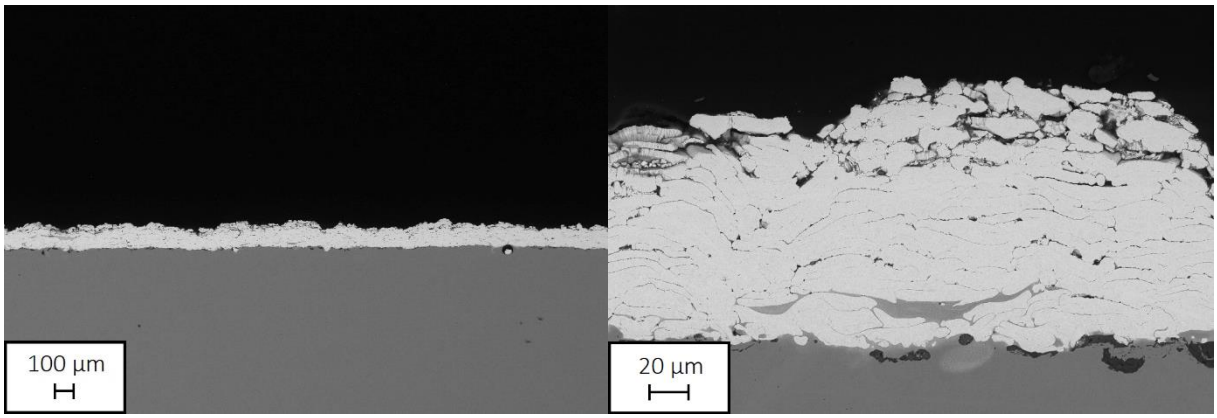

Figure 29: Microstructure of the RF12 coating.

For an easier orientation, the measured values of the porosity and thickness of all samples are summarized in Table 2.

Table 2: Measured porosity of the samples RF1–RF12.

Sample	RF1	RF2	RF3	RF4	RF5	RF6	RF7	RF8	RF9	RF10	RF11	RF12
Porosity (%)	41.4	34.2	32.3	16.7	10.8	7.4	23.0	10.8	10.2	4.8	7.0	7.0
Thickness (µm)	1050	360	925	380	780	325	375	150	405	130	215	110

4.2 Discussion

As the deposited tungsten coatings are planned to be used as an enhancement of the PFC, they should be dense/non-porous, adequately thick (>200 µm) and exhibit good interface quality with the substrate. As shown in the previous studies, there is a rough correlation between thermal conductivity of the coatings and their porosity [31] [32]. Therefore, the optimization of the deposition process was performed with the use of two different powders to possibly obtain results with favorable properties for fusion applications. A total of twelve samples were deposited and, as described further, high quality coatings were obtained after the optimization process.

4.2.1 Optimization of the parameters

For the first deposition RF1, parameters were set according to the previous studies focused on the deposition of tungsten coatings [31] [32]. However, the first sample showed many unmelted particles as well as high porosity (41.4%), which could have been the consequence of the insufficient enthalpy of the plasma for the relatively bigger P1 powder particles. Therefore, halving the feed rate of the powder was suggested at first as this way, the same amount of the plasma enthalpy can be distributed among a smaller amount of material, hence achieving their more proper melting. This step has led to a small improvement only, as the coating on the sample RF2 showed a lesser, but still rather high porosity (34.2%) and almost the same content of unmelted particles. In other words, the coatings RF1 and RF2 did not show properties that would make them applicable as PFC enhancement.

For further improvement, another adjustment was suggested. As the carrier gas contributes to the plasma generation in RF-ICP only partially, its non-ionized, cold proportion partially absorbs the plasma jet enthalpy, leaving a somewhat reduced heat for the powder particles melting. For that reason, reducing the flow of the argon carrier gas was suggested, from 8 slpm to 6 slpm. This adjustment proved to be a step forward, as the coating RF3 showed a reduced occurrence of unmelted particles as well as a lower porosity (32.3%) in comparison with RF1. A lamellar structure made by well-merged splats was observable near the mutual interface coating-substrate, and with increasing distance to the free surface, the splats gradually lose their lamellar shape and appeared poorly deformed. This trend might have been the consequence of the lower layers being gradually deformed by later deposited particles. The lower layers of the coating also solidify under slightly different heat dissipation conditions. RF4 then showed almost no unmelted particles, associated with the use of the reduced Ar flow rate in combination with the reduced powder feed rate. This led to the lowest porosity so far, measured as 16.7%. By a direct comparison of the two influences, it seems that halving the powder feed rate has a greater influence than the reduction of the carrier gas flow rate.

However, the coatings RF3 and RF4 still did not exhibit properties that would make them applicable as PFC enhancement. The particles were still not melted and deformed properly. In fact, rather spherical, poorly deformed particles were observed in the two coatings, probably a consequence of insufficient plasma enthalpy for the used setup. After an in-house modification of the system, it was possible to test the use of helium as the carrier gas instead of argon. As previously mentioned, the carrier gas partially contributes to the plasma generation. Helium is a monoatomic high enthalpy gas, which is typically used to increase the heat capacity of plasma in thermal spraying. Consequently, the use of He turns into higher temperatures of the plasma jet.

For coatings RF5 and RF6, helium was therefore used as the carrier gas. Both coatings showed a dense, lamellar microstructures consisting mainly of well-merged splats within the entire coatings. Coating RF5 showed a good microstructure with low porosity (10.8%). However, a continuous delamination appeared approximately 100 µm above the coating-substrate interface. This might be connected to high density and thickness of the coating, which probably led to residual stresses build-up caused by high difference of the thermal expansion coefficient of the two materials. The RF5 combination is planned to be deposited again to observe if the observed delamination is a perpetual phenomenon occurring invariably. The coating RF6 exhibited an even better microstructure and lower porosity (7.4%), mainly due to the halved powder feed rate. In the case of RF6, no delamination of the coating has been observed. The coating RF6 showed the best results obtained when using the P1 powder and can be considered as good a candidate for further testing.

So far, the best results were achieved with the use of helium as the carrier gas and halved feed rates, which corresponds to the deposition parameters of the sample RF6. Helium is expensive gas, but only a relatively small amount/flow was used in the RF-ICP setup used by us.

Still, the use of helium remains a partially open question, as in the case of a tokamak, it would be necessary to (repeatedly) coat areas corresponding to tens of square meters.

After changing the powder feedstock, coatings RF7 and RF8 were deposited with the same parameters as coatings RF1 and RF2, the worst coatings so far. It turned out that the negative effect of the high flow rate of the Ar carrier gas was not as significant with the use of P2, as both RF7 and RF8 coatings exhibited significantly lower porosity than the samples RF1 and RF2 (23.0% and 10.8% for RF7 and RF8 vs. 41.4% and 34.0% for RF1 and RF2). However, the amount of unmelted particles still remained too high. This leads to a conclusion that the smaller and irregular particles of the powder P2 are more efficient in transferring the plasma enthalpy and are therefore easier to melt. In other words, using the powders with smaller particles might represent a viable pathway in the case of tungsten. This is particularly important given the high melting temperature of tungsten and the limited power of the TekSpray 15 plasma torch.

To follow the same order, coatings RF9 and RF10 were deposited with the same parameters as coatings RF3 and RF4. Coatings RF9 and RF10 proved that reduction of the Ar carrier gas flow is a promising step forward, as we were able to deposit great quality coatings, especially in the case of RF10. In comparison with samples RF3 and RF4 (32.3% and 16.7% porosity), RF9 and RF10 exhibited a significantly better microstructure and a reduced porosity (10.2% and 4.8%). This might have been again associated with the narrower distribution curve of the powder particle sizes and generally smaller particles of the powder P2, as the finer particles were melted more properly in comparison with the coarser (spherical) particles of the powder P1.

To complete the matrix, coatings RF11 and RF12 were deposited with the same parameters as coatings RF5 and RF6, i.e., using helium as the carrier gas. As in the case of RF5 and RF6, the use of helium proved to be a good step, as both coatings RF11 and RF12 showed great microstructure and low porosity (both 7.0%). In the case of sample RF12, the substrate seemed to be partially melted and the free surface showed condensates of evaporated particles. Both these might suggest extensive overheating connected to the increased enthalpy of the plasma and the reduced powder feed rate.

In short, a total of twelve depositions were performed using two different feedstock powders. The deposits ranged from very dense to highly porous (the porosity ranged as much as from 4.8% to 41.4%). Similar levels of porosity in W coatings can be found throughout the literature for different types of thermal spray technologies. While Vassen et al. [33] and Xianliang et al. [34] reached porosity of pure tungsten coatings of around 3% by VPS and RF-ICP, respectively (both exceeding 300 µm thickness), porosities of 4% by APS (Heuer et al. [35]) and even up to 10–15% (Xu et al. [36]) by CAPS were also reported. It can therefore be stated that the optimization done by adjusting the selected parameters (carrier gas type and flow, feed rate and type of powder feedstock) was for the most part successful and our coatings are comparable to those in the literature.

4.2.2 Influence of the powder feed rate

Halving the feed rate proved that regardless of other parameters, reducing the volume of the supplied powder feedstock positively affects the porosity of the coatings. All samples deposited with a halved powder feed rate (blue color bars in Figure 30) exhibited lower porosity than the corresponding samples deposited with a standard feed rate (red color bars in Figure 30). This was more pronounced for the powder P1, which had a higher percentage of bigger particles. In such case, reducing the feed rate resulted into their better melting. Also, in the case of P1, the improvement in the microstructure was most significant for samples deposited with reduced carrier gas flow rate (RF3 and RF4). In the case of P2, halving the feed rate also resulted in obtaining higher quality coatings, which was significant regardless of other parameters (RF8, RF10 and RF12).

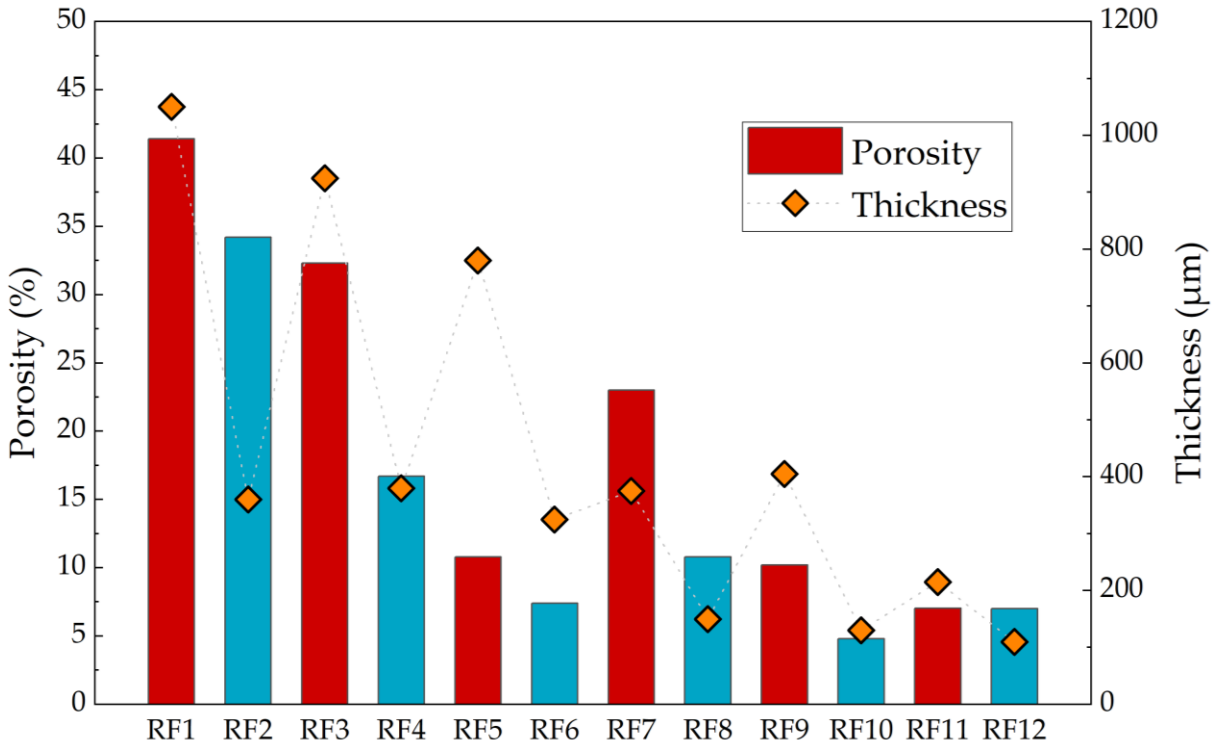

Figure 30: Comparison of porosity of the coatings for standard (red) vs. halved (blue) feed rates. Thickness of the coatings is included as the orange diamonds.

As expected, halving the powder feed rate also lowered the thickness of the (one torch pass) coatings. This change was not linear as the coatings deposited with halved feed rate actually showed less than half the thickness, as it is shown in Figure 30. Nevertheless, the thickness of the coatings can be easily adjusted by performing more passes under the torch, while the economy of the process would increase only slightly. In other words, obtaining thick coatings with lower porosity can be achieved by using the halved feed rates.

4.2.3 Influence of the powder feedstock

The quality and properties of the feedstock powder is a critical factor in thermal spray. For our experiments, the powder P2 seemed to possess more suitable properties than the spherical powder P1. From the obtained results, it is not possible to exactly distinguish whether this was given by its overall smaller particles that are easier to melt in the process, or by their irregular morphology that could trigger an early melting at the edges of the particles. Either way, the use of P2 in general resulted in coatings with better microstructure as compared to those produces from P1.

The influence of narrower distribution and overall smaller particle sizes of the powder P2 was particularly notable when using the reduced Ar flow rate, corresponding to samples RF9 and RF10. In comparison with the corresponding P1 samples RF3 and RF4, RF9 and RF10 exhibited a significantly better microstructure and lower porosity, as shown for clarity in a direct comparison in Figure 31.

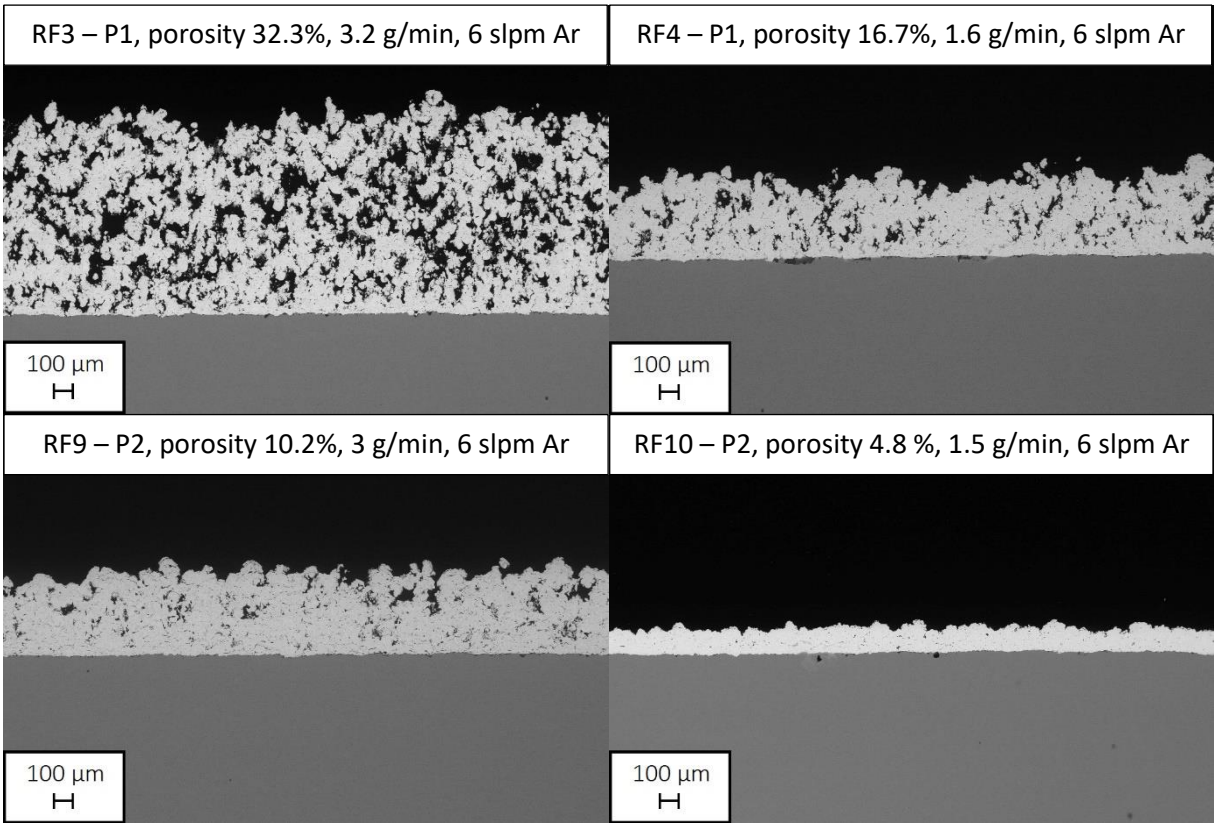

Figure 31: Comparison of microstructure of samples RF3 and RF4 (both from P1), and RF9 and RF10 (both from P2).

4.2.4 Influence of the carrier gas flow rate

As previously mentioned, by reducing the flow rate of the carrier gas, its cooling effect was lowered. With the TekSpray 15 having a limited power, any possible way to increase the plasma enthalpy appeared to be crucial to obtain good quality W coatings. Reducing the flow rate of Ar used as the carrier gas showed to have a great impact on the microstructure, regardless of other spray parameters. The influence of the reduced carrier gas flow rate on the microstructures can be seen in Figure 32, where coatings RF2, RF4, RF8 and RF10 are directly compared. As seen in Figure 32, reducing the Ar flow rate while maintaining other process parameters (powder feedstock and feed rate) resulted in significant decrease in the porosity.

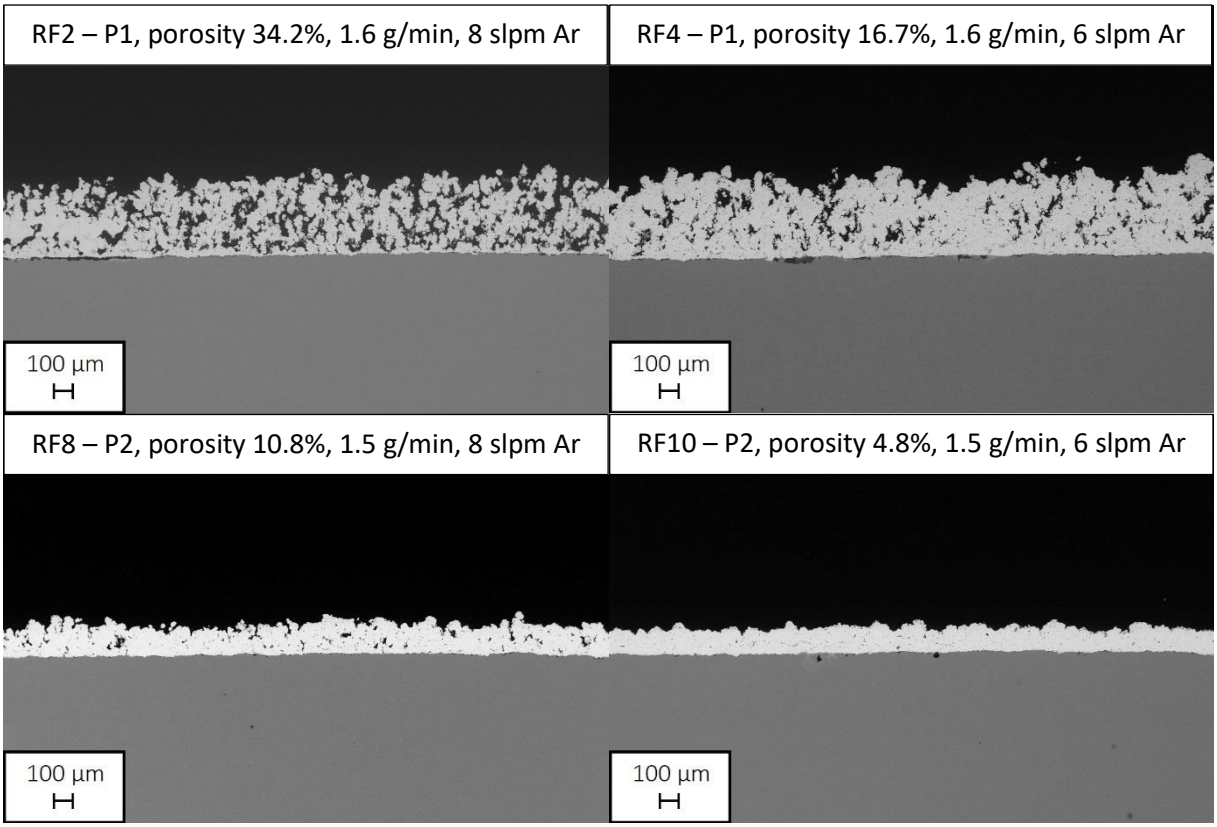

Figure 32: Comparison of microstructure of samples RF2 and RF8 (both 8 slpm Ar) and RF4 and RF10 (both 6 slpm Ar).

4.2.5 Influence of the carrier gas type

The most significant improvement was achieved by deposition with the use of helium as the carrier gas. The use of helium proved to improve the overall quality of the coatings, again regardless of other deposition parameters. This effect can be illustrated by a comparison of coatings RF7 and RF8 (8 slpm Ar) with RF11 and RF12 (8 slpm He), as seen in Figure 33.

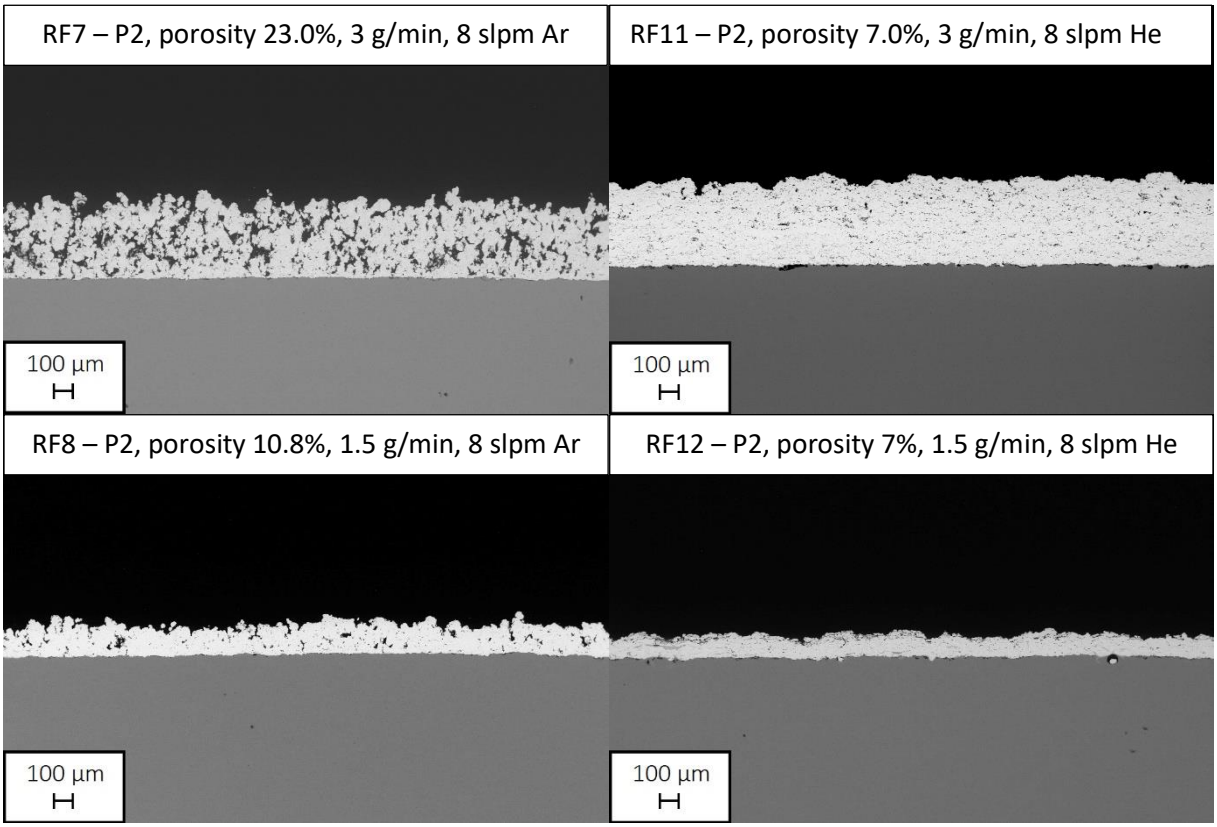

Figure 33: Comparison of microstructure of samples RF7 and RF8 (both 8 slpm Ar) and RF11 and RF12 (both 8 slpm He).

It can be stated that all coatings deposited with the use of He as a carrier gas exhibited good microstructure with low porosity as well as no signs of delamination on the interface coating-substrate. Therefore, these coatings can be considered as suitable candidates for further studies.

5 Conclusions

This thesis aimed to investigate the possibility of deposition of thick, dense tungsten coatings using RF-ICP technology for the potential use in nuclear fusion applications. The influence of the powder feedstock type was determined, as was the influence of the powder feed rate, as well as carrier gas type and its flow rate.

Commonly available steel AISI 304 was chosen as the substrate material for this trial optimization, as it possesses similar properties (especially thermal conductivity) to Eurofer steel planned to be used as a PFC material. Two dissimilar tungsten powders were chosen as the feedstock material. Using these two, a total of twelve coatings were deposited with the process parameters being subsequently optimized.

From the obtained results, it can be concluded that:

- The type of feedstock can change the properties of the deposit coating. A powder with smaller W particles and a narrower distribution results in coatings with lower porosity and more unified microstructure.
- Reduction of the W powder feed rate results in a reduced per-pass thickness of the coatings, but has a strong positive impact on the microstructure of the coatings.
- Reduction of the Ar carrier gas flow increases the coating quality via a reduced enthalpy drain by the introduction of the relatively cool gas.
- The type of the carrier gas has a major impact on the microstructure of the coatings, as generally better results were obtained with the use of (more expensive) He.
- The best results in terms of microstructure and associated porosity and thickness were achieved in the case of samples RF6 (P1, He carrier gas, halved feed rate), RF10 (P2, reduced Ar flow rate, halved feed rate), RF11 (P2, He carrier gas, standard feed rate) and RF12 (P2, He carrier gas, halved feed rate).

In summary, RF-ICP shows a promising potential for deposition of W coatings for fusion applications. From the obtained results, two pathways appear to be viable solution to getting good quality deposits – preparing the coatings with reduced Ar flow rate (RF10), or using the more expensive He (RF6, RF11 and RF12). Aside from these, further optimization of the deposition process is planned. This involves other, not-yet tested parameters (such as, e.g., stand-off distance of the torch from the substrates or the cooling intensity by variations in the sample holder revolutions) as well as a third W powder feedstock. This should be followed by a deposition on substrates made from material planned to be used as PFC, the Eurofer steel.

6 List of images

7 Bibliography

[1] RIPA, M., MLYNAR, J., ZACEK, F., WEINZETTL, F. Řízená termojaderná fúze pro každého. ÚFP AV ČR, Prague, 2011. ISBN 80-902724-7-9.

[2] PANETH, F., PETERS, K. Über die Verwandlung von Wasserstoff in Helium. Naturwissenschaften, 1926, 14.43: 956-962.

[3] ENTLER, S. Jaderná fúze–budoucnost energetiky. Energetika, 2015, 3: 136.

[4] MLYNAR, J. ITER: cesta ke zvládnutí řízené termonukleární fúze. Pokroky matematiky, fyziky a astronomie, 2004, 49.2: 129-150.

[5] ENTLER, S., MLYNAR, J. Spoutání slunce. Středisko společných činností AV ČR, vvi, 2016. ISBN 978-80-270-0252-8.

[6] MOHR, S., WARD, J. Helium production and possible projection. Minerals, 2014, 4.1: 130-144.

[7] HAMERLY, R. Inertial Confinement Fusion. Stanford University, 2010.

[8] DUBUS, G. D. From plain visualisation to vibration sensing: using a camera to control the flexibilities in the ITER remote handling equipment. 2014.

[9] MCCRACKEN, G., STOTT, P. Fúze: energie vesmíru. Mladá fronta, Praha, 2006. ISBN 80-204-1453-3.

[10] LAWSON, J. D. Some criteria for a power producing thermonuclear reactor. Proceedings of the physical society. Section B, 1957, 70.1: 6.

[11] ARTSIMOVICH, L. A. Tokamak devices. Nuclear Fusion, 1972, 12.2: 215.

[12] SMIRNOV, V. Tokamak foundation in USSR/Russia 1950–1990. Nuclear fusion, 2009, 50.1: 014003.

[13] ENTLER, S., MLYNAR J., DOSTAL V. Základy fúzní energetiky IV: Jaderné komponenty [online]. [cit. 2023-04-10]. Dostupné z: https://energetika.tzb-info.cz/elektroenergetika/14669-zaklady-fuzni-energetikyiv-jaderne-komponenty

[14] ITER: Machine [online]. ITER Organization [cit. 2023-04-10]. Dostupné z: www.iter.org/mach

[15] FEDERICI, G., BIEL, W., GILBERT, M.R., KEMP, R., TAYLOR, N., WENNINGER, R. European DEMO design strategy and consequences for materials. Nuclear Fusion, 2017, 57.9: 092002.

[16] CARDARELLI, F. Materials handbook: a concise desktop reference. 2008.

[17] LASSNER, E., SCHUBERT, W. Tungsten: properties, chemistry, technology of the elements, alloys, and chemical compounds. Springer Science & Business Media, 1999.

[18] SIEGMANN, S., ABERT, Ch. 100 years of thermal spray: About the inventor Max Ulrich Schoop. Surface and Coatings Technology, 2013, 220: 3-13.

[19] MUSALEK, R. Inženýrské výzvy v oblasti žárového stříkání. 2011.

[20] DIN EN 657:2005-06. Thermal spraying - Terminology, classification. 2005.

[21] WANK, A. Basics of thermal spray technology. GTV Verschleiss-Schutz GmbH: Luckenbach, Germany, 2006.

[22] ZAVAREH, M. A., SARHAN A. A. D. M., ZAVAREH P. A., RAZAK B. A., KAKOOEI, S. Fundamentals and applications of thermal spray coating. Can. J. Basic Appl. Sci, 2017, 5: 1-11.

[23] FLAME SPRAY TECHNOLOGIES (FST), Dijkgraaf 40, 6921RL Duiven, The Netherlands. Science+Business Media, LLC, 2013, ISBN 978-0-387-28319-7.

[24] COTELL, C. M., SMIDT, F. A. Thermal spray coatings. ASM Handbook, 2002, 5: 497-509.

[25] BOULOS, M. I. New frontiers in thermal plasmas from space to nanomaterials. Nucl. Eng. Technol., 2012.

[26] DAVIS, J. R. Handbook of thermal spray technology. ASM international, 2004.

[27] VUORISTO, P. Thermal spray coating processes. In: Comprehensive materials processing, 1st edition Volume 4: Coatings and films. Elsevier, 2014. p. 229-276.

[28] WIGREN, J. Grit blasting as surface preparation before plasma spraying. Surface and Coatings Technology, 1988, 34.1: 101-108.

[29] TEKNA. TekSpray 15 Operating manual. Sherbrooke, Quebec, 2000.

[30] ZLATNIK, R. Analýza parametrů podávání práškových materiálů v technologii RF-ICP. 2018.

[31] KLECKA, J., CIZEK, J., MATEJICEK, J., LUKAC, F., ZLATNIK, R., CHRASKA, T. Tailoring the structure of RF-ICP tungsten coatings. Surface and Coatings Technology. 2021, 406: 126745.

[32] KLECKA, J., CIZEK, J., MATEJICEK, J., ZLATNIK, R. Optimization of RF-ICP tungsten deposits for plasma facing components. In: Proc. Intl. Conf. Nuclear Energy for New Europe, Portoroz, Slovenia. 2018.

[33] VAßEN, R., RAUWALD, K. H., GUILLON, O., AKTAA, J., WEBER, T., BACK, H. C., QU, D., GIBMEIER, J. Vacuum plasma spraying of functionally graded tungsten/EUROFER97 coatings for fusion applications. Fusion engineering and design, 2018, 133: 148-156.

[34] XIANLIANG, J., GITZHOFER F., BOULOS M. I. Thermal spray coating of tungsten for tokamak device. Plasma Science and Technology, 2006, 8.2: 164.

[35] HEUER, S., MATEJICEK, J., VILEMOVA, M., KOLLER, M., ILLKOVA, K., VEVERKA, J., WEBER, T., PINTSUK, G., COENEN, J. W., LINSMEIER, CH. Atmospheric plasma spraying of functionally graded steel/tungsten layers for the first wall of future fusion reactors. Surface and coatings technology, 2019, 366: 170-178.

[36] XU, Y., HIROOKA, Y., NAGASAKA, T., YAGI, J. Hydrogen gas-driven permeation through F82H steel coated with vacuum plasma-sprayed tungsten. Plasma and Fusion Research, 2016, 11: 2405064-2405064.

8 List of symbols and abbreviations

Symbols

m [kg]	Mass
η [kg·m^{-3}]	Density of atomic nuclei
τ_E [s]	Energy confinement time of the atomic nuclei
P [W]	Power
ρ [kg/m^3]	Density
T [K]	Temperature

Abbreviations

APS	Atmospheric plasma spray
CAPS	Controlled atmosphere plasma spray
CFC	Composite Fiber Co-extrusion
CVD	Chemical vapor deposition
D	Deuterium
DC	Direct current
DEMO	Demonstration power plant
DGS	Detonation gun spray
HVOF	High-velocity oxy fuel
ICP-MS	Inductively-coupled plasma – mass spectrometry
ICP-OES	Inductively-coupled plasma – optical emission spectrometry
ITER	International Thermonuclear Experimental Reactor
JET	Joint European Torus
NBI	Neutral beam injection
PFC	Plasma facing components
PVD	Physical vapor deposition
RF-ICP	Radio frequency inductively-coupled plasma
SEM	Scanning electron microscope
T	Tritium
TMP	Torus with a magnetic field
VPS	Vacuum plasma spray

9 List of publications

Journal papers

J. Cizek, J. Klecka, L. Babka, R. Musalek, H. Hadraba, J. Kondas, R. Singh, M. Pazderova: Protective Mo and Fe Coatings by CS and RF-ICP for PbLi Coolant Environments in Generation IV Fission Reactors. Journal of Thermal Spray Technology 32, 363–374, 2023.

Conference papers

J. Cizek M. Vilemova F. Lukac J. Klecka L. Babka H. Hadraba, J. Kondas, R. Singh, M. Pazderova: Protective CS deposits in nuclear sector: W and W-Cr for fusion + Fe/Mo for Gen IV fission. Workshop on thermal spray coatings technologies and characterization, 2023, Pilsen

J. Cizek, J. Klecka, L. Babka, H. Hadraba, J. Kondas, R. Singh, M. Pazderova: Protective coatings for liquid metal cooled reactors. Les Rencontres Internationales sur la Projection Thermique, 2022, Julich.

L. Babka, J. Cizek, J. Klecka, H. Hadraba, J. Kondas, R. Singh, M. Pazderova: Thick protective Fe and Mo coatings for PbLi coolant environments prepared by RF-ICP and cold spray. International Conference Nuclear Energy for New Europe, 2022, Portoroz.

J. Cizek, J. Klecka, L. Babka, J. Kondas, R. Singh, M. Pazderova: Protective Mo and Fe coatings by CS and RF-ICP for PbLi coolant environments in generation IV fission reactors. International Thermal Spray Conference, 2022, Vienna, Austria.

J. Cizek, J. Klecka, L. Babka: Thick protective Fe coatings for PbLi coolant environments. International Conference Nuclear Energy for New Europe, 2021, Bled, Slovenia.